KTH Electrical Engineering

Cooperative Multi-Vehicle Circumnavigation and Tracking of a Mobile Target

JOANA FILIPA GOUVEIA FONSECA

Licentiate Thesis

Stockholm, Sweden 2020

KTH School of Electrical Engineering and Computer Science
Division of Decision and Control Systems
SE-100 44 Stockholm
SWEDEN

TRITA-EECS-AVL-2020:14
ISBN 978-91-7873-446-7

Akademisk avhandling som med tillstånd av Kungliga Tekniska högskolan framläges till offentlig granskning för avläggande av teknologie licentiatexamen i elektro- och systemteknik onsdagen den 13 mars 2020 klockan 10.00 i sal F3, Kungliga Tekniska högskolan, Lindstedtsvägen 26, Stockholm.

Tryck: Universitetsservice US AB

Abstract

A multi-vehicle system is composed of interconnected vehicles coordinated to complete a certain task. When controlling such systems, the aim is to obtain a coordinated behaviour through local interactions among vehicles and the surrounding environment. One motivating application is the monitoring of algal blooms; this phenomenon occurs frequently and has a substantial negative effect on the environment such as large-scale mortality of fish. In this thesis, we investigate control of multiple unmanned surface vehicles (USVs) for mobile target circumnavigation and tracking, where the target can be an algal bloom area. A protocol based on local measurements provided by the vehicles is developed to estimate the target's location and shape. Then a control strategy is derived that brings the vehicle system to the target while forming a regular polygon.

More precisely, we first consider the problem of tracking a mobile target while circumnavigating it with multiple USVs. A satellite image indicates the initial location of the target, which is supposed to have an irregular dynamic shape well approximated by a circle with moving center and varying radius. Each USV is capable of measuring its distance to the boundary of the target and to its center. We design an adaptive protocol to estimate the circle's parameters based on the local measurements. A control protocol then brings the vehicles towards the target boundary as well as spreads them equidistantly along the boundary. The protocols are proved to converge to the desired state. Simulated examples illustrate the performance of the closed-loop system.

Secondly, we assume that the vehicles can only measure the distance to the boundary of the target and not to its center. We propose a decentralised least-squares method for target estimation suitable for circular targets. Convergence proofs are given for also this case. An example using simulated algal bloom data shows that the method works well under realistic settings.

Finally, we investigate how to extend our protocols to a quite general irregular mobile target. In this case, each vehicle communicates only with its two nearest neighbors and estimates the curvature of the target boundary using their collective measurements. We validate the performance of the protocol under various settings and target shapes through a numerical study.

Sammanfattning

Multi-fordon-styrsystem består av sammankopplade fordon som koordinerar för att slutföra en given uppgift. I sådana styrsystem är målet att få ett koordinerat beteende via lokala interaktioner mellan fordonen och miljön de vistas i. Ett motiverande exempel är övervakning av algblomning, ett fenomen som inträffar frekvent och har omfattande negativa effekter såsom kraftig mortalitet hos fiskar. I denna rapport undersöker vi hur Unmanned Surface Vehicles (USVs) kan styras för att cirkulera och spåra ett givet mobilt objekt, till exempel en yta med algblomning. Ett protokoll är utvecklat för att estimera det mobila objektets position och form, baserat på lokala mätningar utförda av fordonen, samt en reglerstrategi tas fram som styr systemet med fordon till objektet samtidigt som de formar en regelbunden polygon.

Mer precist undersöker vi först problemet att samtidigt spåra och cirkulera ett mobilt objekt med USVs. En satellitbild indikerar startpositionen av objektet, antaget att ha en irreguljär tidsvarierande form som kan approximeras väl av en cirkel med tidsberoende center och radie. Varje USV kan mäta avståndet till objektets rand och center. Vi designar ett adaptivt protokoll för att estimera cirkelns parametrar baserat på lokala mätningar. Ett reglerprotokoll styr sedan fordonen mot objektets rand samt sprider ut dem ekvidistant kring randen. Vi bevisar att protokollen konvergerar mot önskat tillstånd. Två simuleringar visar det slutna systemets prestanda.

Sedan antar vi att fordonen endast kan mäta avståndet till randen på objektet, men inte tills dess center. Vi tar fram en decentraliserad minstakvadratmetod för att estimera objektet, lämpligt för cirkulära objekt. Konvergens bevisas även i detta fall. Ett exempel med data från en simulerad algblomning visar att metoden fungerar bra under realistiska scenarion.

Slutligen undersöker vi hur protokollen kan vidareutvecklas för mobila objekt med tämligen generella irreguljära former. I detta fall antar vi att fordonen endast kan kommunicera med sina två närmaste grannar och estimera kurvan för objektets rand från deras samlade mätningar. Vi validerar protokollen via två simuleringar.

Acknowledgements

I'm very thankful to have Professor Karl Henrik Johansson as my supervisor. Thank you for the opportunity to work in this lively team and on such a relevant and exciting research topic. I admire your ability to create a strong, safe and cooperative working environment that allows us to thrive! Thank you for your expertise, your kindness, support and understanding. I always leave our meetings less anxious than when I get in.

Thanks also to my co-supervisor Jonas Mårtensson. It has been great to work with you on Nonlinear Control course, I learnt a lot from it and it's so encouraging to see all the commitment and energy you put into creating it. I want to thank Jieqiang Wei for helping me a lot in the beginning of my PhD, I learnt a lot from you. Thank you for your positive energy every day and your inside tips! I'm also very glad to work with Tor Arne Johansen from NTNU. Thank you for your real world implementation knowledge and your sharp points on our work. Thank you so much to everyone else who also proof-read part of this thesis: Pian Yu, Matin Jafarian, Philip Pare and Yuchao Li. Och tack Elis Stefansson för att du skrev mitt Sammanfattning.

I want to thank this division as a whole, each and every one of you for making my workplace a place I look forward to go to every day. I want to thank particularly my office mates for making it the coolest office. I didn't want to have anyone feeling left out and I'm afraid there are not enough lines in one page to state all of your names but there is enough space in my heart for all of you!

Heartfelt thanks to two very special women with whom I've shared plenty and whose strength and intelligence I admire so much. Mina and Matin, I wish to be so lucky as to continue sharing glasses of wine with you both.

Many thanks to my Porto family. Thanks dad for the constant love and support and thank you Ana and Marta, for inspiring me.

This work is partially supported by the Knut and Alice Wallenberg Foundation, the Swedish Research Council, and the Swedish Foundation for Strategic Research.

Jo ♡

Contents

Chapter 1

Introduction

A multi-vehicle system is composed of interconnected vehicles coordinated to complete a certain task. Each vehicle has its own dynamics and communicates with a subset of the other vehicles, possibly influencing each other's decisions. Multi-vehicle systems have been the subject of an enormous body of research over the past few decades. The reason for such interest is often their robustness, lower price, and efficiency compared to a more complex, and expensive single vehicle. Multi-vehicle systems are sometimes inspired by multi-organism partnerships, for example, ants building an underground home, birds flying energy efficiently or even humans working together on a project. Multi-vehicle systems, for example, systems of unmanned surface vehicles (USVs) can be applied to monitor harmful algal blooms in the Baltic and Norwegian seas. These algal blooms pose a threat to the environment and human health and, therefore, there is a growing need to study their evolution in real-time.

The rest of this chapter is organised as follows. In Section 1.1, we present our motivation for multi-vehicle tracking of mobile targets by considering the phenomenon of harmful algal blooms. In Section 1.2, we formulate the main problem considered in the thesis. The outline of the thesis and the related contributions are presented in Section 1.3.

1.1 Motivation

All over the world, the phenomena of harmful algal blooms as seen in Fig. 1.1 occurs frequently and with increasing impact. It has a substantial negative effect on the environment and human health. Therefore, plenty of research has been done regarding the nature of this phenomena, its causes, and impact. For example, the Swedish Meteorological and Hydrological Institute (SMHI) has been documenting algal blooms in the Baltic sea via satellite and monthly missions of a manned research vessel for around 20 years [1]. In this thesis we suggest a novel approach to monitor algal blooms and other biological phenomena at sea. Our approach

Figure 1.1: Satellite sensor MODIS (Moderate Resolution Imaging Spectroradiometer) provided satellite picture showing algal blooms in the Baltic Sea in July 2005. (Courtesy of SMHI)

includes a satellite paired with a multi-vehicle system that should circumnavigate and estimate the algal bloom motion.

Harmful algal blooms is a phenomenon where plankton algae grows rapidly and form very large populations in a short period of time. Algal blooms occur in all types of water: at sea, around the coast, in lakes, and streams, both in Sweden and abroad. Usually, algal blooms can be found mostly near the water surface because the sunlight is strongest there. According to [2], algal blooms cause human illness, large-scale mortality of fish, shellfish, mammals, birds, and deteriorates water quality. Important questions are why these phenomena occur and why they have been growing over the past years. One of the reasons is climate change as discussed in [3]. In that study, they infer that climate change will influence marine planktonic systems globally, and that it is conceivable that algal blooms may increase in frequency and severity. Higher temperatures and ocean stratification are beneficial for algal bloom species. Also mentioned in [3], agricultural practices and other land usages are important.

There are many studies on dynamical modelling of algal blooms. There has been simulation studies of the dynamics of algal blooms, more specifically diatoms and flagellates which are two species of algal blooms. Throughout this thesis, we will use SINTEF's numerical ocean model simulation system called SINMOD. Fig. 1.2 shows a snapshot of a SINMOD simulation of flagellates near the Norwegian sea coast. Here, each pixel is about 100 meters so the image is about 35km in longitude and 18km in latitude. Also, we consider, for example, that an algal bloom exists

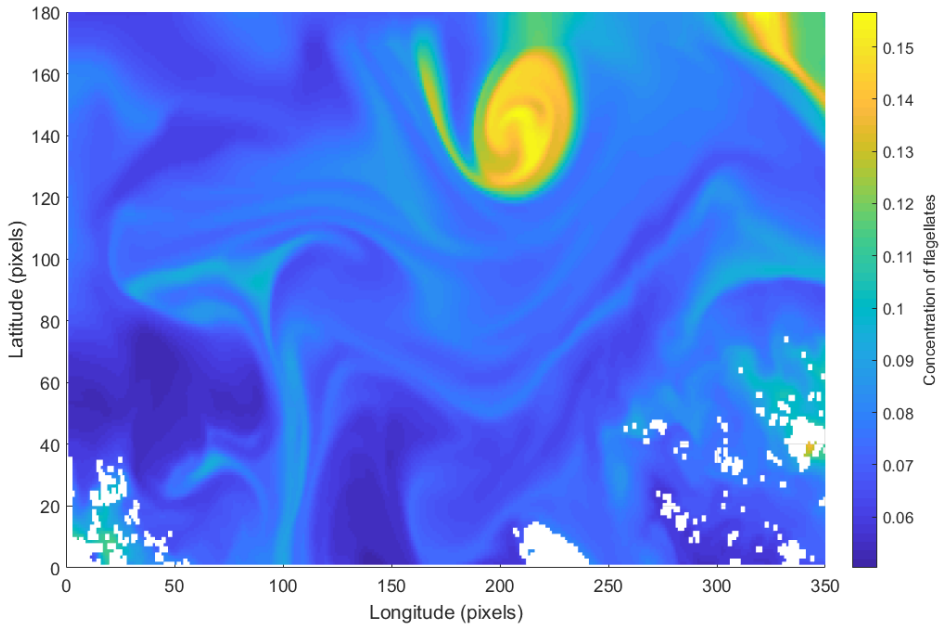

Figure 1.2: SINMOD simulation of concentration of flagellates in the Norwegian sea. (Courtesy of SINTEF)

from the concentration level of 0.13 or above. In that case, there is an algal bloom shape in the upper center of the figure as well as a part of another algal bloom shape on the upper right corner. In most results, this simulated abundance and distribution of diatoms and flagellates changes remarkably not only during the highly dynamic spring bloom but also during the summer [4]. In [5], it is stated that future advances in modelling will occur through the junction of models and data, using data to conceptualise models and using models to understand data. This chapter reviews many types of dynamical models that are available and the need for modelling harmful algal blooms.

Currently, there are a few approaches to solve the problem of algal bloom data collection and modelling. We will present two of the most interesting methods by SMHI: the first one via satellite and the second one via monthly missions on a manned research vessel.

Via satellite, SMHI has been monitoring the algae situation since 2002 through the Baltic Algae Watch System [6]. This is a satellite-based monitoring system for blue-green (cyanobacteria) algal blooms in the Baltic Sea. Fig. 1.3 represents the data SMHI collected in the summer of 2019, available on their website. Comparing the data from the two consecutive days illustrates how noisy and unpredictable the algal blooms can be. In the left image we can see most of the Baltic sea and thus

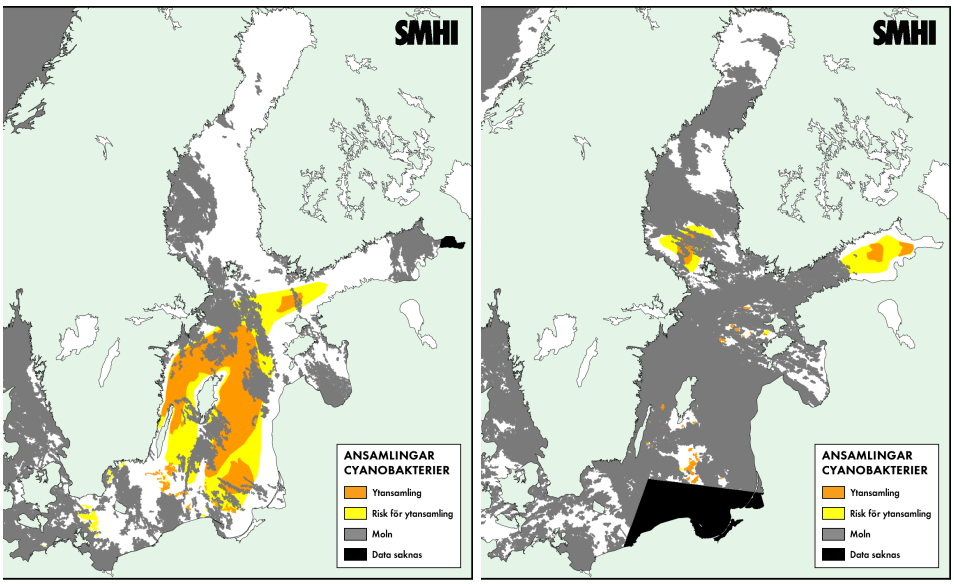

Figure 1.3: Satellite data collected by SMHI. Left: Taken on the 5th of August 2019. Right: Taken on the 6th of August 2019. Legend: Orange for high algae concentration; yellow for risk of high algae concentration; grey for presence of clouds; and black for data missing. (Courtesy of SMHI)

infer the location of the algal blooms. However in the right image, one day after, we can barely locate the algal blooms, for instance, off the coast of Stockholm. This difficulty is caused by the presence of clouds, a common occurrence in this region of the world.

Via a research vessel, local measurements are taken using a long list of sensors and a team of researchers. The procedure and results of each mission are detailed in a report. Fig. 1.4 represents one mission, found in the 7th report of 2019 [7]. This figure represents the plan for data collection including fixed monitoring stations as well as defined collection points through which the research vessel would pass and collect data.

We propose a novel approach that seeks to provide frequent, reliable, and local measurements of algal blooms. The solution we provide seeks to substitute this expensive manned mission that occurs once a month with a more affordable, continuous, and autonomous option. We wish to provide a multi-vehicle setup using vehicles such as the USV from KTH as seen in Fig 1.5 and an algorithm capable of autonomously following and enclosing algal blooms. Therefore, we believe that we can improve the amount and quality of data collected by using a multi-vehicle system. Since algal blooms can be found mostly near the water surface, we focus on satellite as well as surface and aerial vehicles.

Figure 1.4: SMHI's research vessel mission on the 7th report of 2019. Legend: Red for high frequency of data collection; dark blue for monthly data collection; light blue for nutrient mappings; and the black line for the vessel's trajectory. (Courtesy of SMHI)

1.2 Problem formulation

The problem we consider in the thesis is how to develop estimation and control protocols so as to track a mobile target while circumnavigating it with multiple USVs. We consider a system as shown in Fig. 1.6 composed of a satellite capable of providing noisy and cloudy images twice a day to a team of surface vehicles. The surface vehicles have a GPS receiver as well as various types of sensors. The algal bloom shape to track may be static or dynamic. Changes may occur at a fast or slow pace, according to factors like the wind, temperature, ocean currents, etc.

This thesis considers the following questions:

1. How to control multiple USVs to a desired formation?

Figure 1.5: Four USVs "duckling" used in [8]

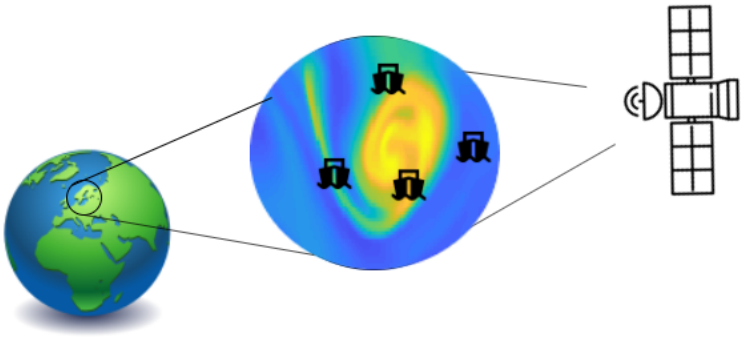

Figure 1.6: Tracking an algal bloom using a multi-vehicle system with local sensors and a satellite

2. How to estimate a mobile target with time-varying shape?
3. How to circumnavigate a mobile target over time?
4. Can we guarantee convergence to the shape in a regular polygon formation for all time?

Chapters 3 and 4 answer Questions 1, 2, 3, and 4 with estimation and circumnavigation protocols that guarantee convergence towards a circular target in a regular polygon formation. Chapter 5 answers to Questions 1, 2, and 3 with estimation and circumnavigation protocols for general non-circular shapes without convergence guarantees.

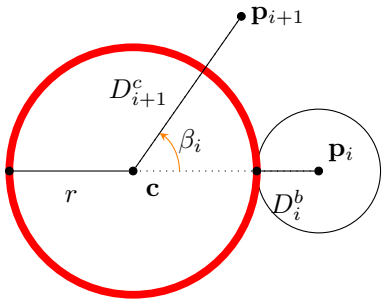

Figure 1.7: Scheme of the estimated $\mathbf{c}$ and r as well as the angle β_i between two agents at positions $\mathbf{p}_{i+1}$ and $\mathbf{p}_i$.

The shape tracking and circumnavigation problem includes three sets of variables: system state variables, measurement variables, and estimated variables. The variables for the state of the system are the position and velocity of each vehicle defined as $\mathbf{p}_i$ and $\dot{\mathbf{p}}_i$, for $i = 1, \ldots, n$, respectively, where n is the number of vehicles. The estimated variables are the variables we obtain after estimating the location, size or curvature of the target and are defined as the center $\mathbf{c}$ and the radius r. The measurement variables are with respect to the distance of a vehicle to the target. We define the distance to the center of the target as D^c_i and the distance to the boundary of the target D^b_i. We also define the angle between agent i and agent $i+1$ as β_i, depicted in Fig 1.7.

Throughout this thesis we seek to design control protocols as a function of the current state, the measurements taken and the estimates or references calculated:

$$\mathbf{u_i} = f(\mathbf{p}_i, \mathbf{p}_{i+1}, \hat{\mathbf{c}}, \hat{r}, D^c_i, D^b_i)$$

We also design an estimation algorithm to compute $\hat{\mathbf{c}}$ and $\hat{r}$ based on $\mathbf{p}_i$, $\mathbf{p}_{i+1}$, $\mathbf{c}$, r, D^c_i, and D^b_i.

The problem we consider is how to choose the control law and the estimator to guaranteee convergence to the boundary of the target and that the USVs are equally spaced along the boundary.

Fig. 1.8 shows how four USVs sucessfully track an algal bloom target. Notice how the vehicles are on top of the boundary within a small bound as well as equally spread across the shape.

1.3 Thesis outline and contributions

In this section, we provide an overview of the thesis. We describe each chapter's contents and contributions and we indicate the publications upon which they are based.

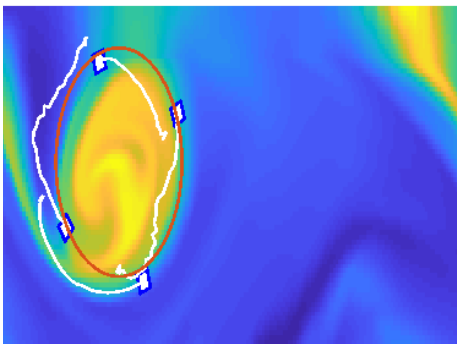

Figure 1.8: Example of a system of 4 vehicles tracking an algal bloom shape.

Chapter 2: Background

In Chapter 2, we provide the background of the thesis by analysing related literature. Firstly, we discuss how multi-vehicle systems have been relevant for marine sensing and which vehicle systems have been used for different marine sensing applications. Then, more specifically, we review how cooperative circumnavigation has been used for target tracking. We relate these contributions to our own, in the present thesis, by comparing assumptions, methods, and applications.

Chapter 3: Cooperative circumnavigation using adaptive estimation

In Chapter 3, we consider the problem of tracking a mobile target using adaptive estimation while circumnavigating it with a system of USVs. The mobile target considered is an irregular dynamic shape approximated by a circle with moving center and varying radius. The USV system is composed of n USVs of which one is equipped with an UAV capable of measuring both the distance to the boundary of the target and to its center. The USV equipped with the UAV uses adaptive estimation to calculate the location and size of the mobile target. The USV system must circumnavigate the boundary of the target while forming a regular polygon. We design two algorithms: One for the adaptive estimation of the target using the UAVs measurements and another for the control protocol to be applied by all the USVs in their navigation. The convergence of both algorithms to the desired state is proven up to a limit bound. Two simulated examples are provided to verify the performance of the algorithms designed.

This chapter is based on the following contribution:

- J. Fonseca, J. Wei, K. H. Johansson, and T. A. Johansen, "Cooperative circumnavigation for a mobile target using adaptive estimation". Submitted to CONTROLO 2020, Braganca, Portugal.

Chapter 4: Cooperative circumnavigation with distributed sensing

In Chapter 4, we propose a reliable method to track algal blooms using a set of USVs. A satellite image indicates the existence and initial location of the algal bloom for the deployment of the robot system. The algal bloom area is approximated by a circle with time varying location and size. This circle is estimated and circumnavigated by the robots which are able to locally sense its boundary. A multi-agent control algorithm is proposed for the continuous monitoring of the dynamic evolution of the algal bloom. The algorithm is comprised of a decentralised least squares estimation of the target and a controller for circumnavigation. We prove the convergence of the robots to the circle, in equally spaced positions around it. Simulation results with data provided by the SINMOD ocean model are used to illustrate the theoretical results.

This chapter is based on the following contribution:

- J. Fonseca, J. Wei, K. H. Johansson, and T. A. Johansen, "Cooperative decentralized circumnavigation with application to algal bloom tracking", in IEEE/RSJ International Conference on Intelligent Robots and Systems, 2019.

Chapter 5: Cooperative circumnavigation of non-circular shapes

In Chapter 5, we consider the problem of tracking an irregular shape using a decentralized system of vehicles as well as circumnavigating such shape. Similar to the previous chapter, we propose a protocol based on decentralized least squares estimation. Each vehicle can only communicate with its nearest neighbours, thus forming an undirected ring graph. We assume that each vehicle measures its distance to the boundary of the target as well as whether it is inside or outside such target. The convergence of both algorithms to the desired state is proven up to a limit bound. Two simulated examples are provided to verify the performance of the algorithms designed.

This chapter is based on the following contribution:

- J. Fonseca, J. Wei, K. H. Johansson, and T. A. Johansen, "Cooperative decentralised circumnavigation of irregular moving shapes with nearest neighbour communication". In preparation.

Chapter 6: Conclusions and Future Work

Finally, in Chapter 6, we conclude the present thesis with a summary and discussion of the results as well as with directions for future work, indicating some planned extensions of this thesis.

Contribution by the author

The order of the author names reflects the workload, where the first has the most important contribution. In all listed publications, all authors were actively involved

in formulating the problems, developing the solutions, evaluating the results, and writing the papers.

Chapter 2

Background

This chapter provides a literature review of the thesis. We present some examples of the usage of various multi-vehicle systems for marine sensing applications. We also discuss why these systems are common in marine sensing. An important topic within multi-vehicle systems is formation control. In particular, we discuss literature on cooperative circumnavigation and target tracking.

2.1 Multi-vehicle control for marine sensing

Multi-vehicle control is frequently used for marine sensing applications. Marine sensing is a field that has been growing over the past years as the need for ocean monitoring has become more important. Unmanned vehicles have been recognised to allow higher levels of precision and cost efficiency in many research expeditions [9]. As a result, control of multi-vehicle systems presents itself as an essential component to the problem of marine sensing.

Marine sensing is one of this decade's prominent investments. There is a need for a sustained, persistent, and affordable presence in the oceans. Oceans cover 96% of the Earth thus making ocean observation a problem on truly planetary scale. This problem is of particular importance to countries with a high percentage of ocean territory, such as Portugal, as depicted in Fig. 2.1.

In a book on the future of the Portuguese ocean, Sousa et al. [10] describe that constant ocean monitoring is necessary albeit not an easy task. They claim that some of the key applications are the understanding and the monitoring of climate change, ocean acidification, unsustainable fishing, pollution, waste, loss of habitats, biodiversity, shipping, security, and mining. They further claim that such goals can only be achieved by *an incremental and multi-dimensional approach* including two steps: First, an increase in the number of systems in operation in the oceans with new fleets of robotic vehicles of unprecedented spatial and temporal resolution. Second, networking existing systems and new robotic vehicle systems for coordinated

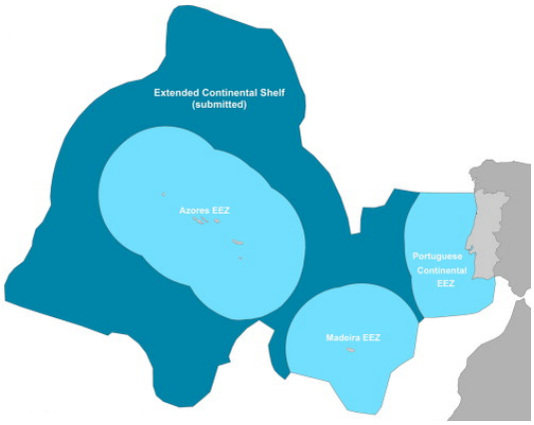

Figure 2.1: Portuguese ocean and land territory.

adaptation to observational needs. An illustration of such a system is represented in Fig. 2.2.

Unmanned vehicles are particularly relevant in challenging or hazardous environments, and if real-time data exchange is required [11]. In [12] it is stated that autonomous systems are becoming more powerful and utilise the capabilities of several types of devices such as Unmanned Aerial Vehicles (UAVs), Unmanned Surface Vehicles (USVs) and Autonomous Surface Vehicles (ASVs). ASVs allow to perform a series of measurement runs over a long period of time at sea [13].

Multi-vehicle systems present many control challenges. The benefits that cooperative multi-vehicle systems offer have inspired extensive research efforts. Murray [15] discusses multi-vehicle systems challenges as the uncertainty caused by inter-vehicle communications and distributed operation, system complexity due to the problem size and coupling between tasks, and scalability to a potentially large collection of vehicles. More recently, Cao et al. [16] define four main directions of research: consensus, formation control, optimisation, and estimation.

2.2 Cooperative circumnavigation for target tracking

Cooperative circumnavigation for target tracking is a particular problem within cooperative multi-vehicle control. The literature on this topic is, in fact, quite extensive and spans over 20 years of research. Some examples are formation control or cooperative circumnavigation of a known target, formation and estimation for tracking a moving target defined as a unit point and finally, more recently, estimation protocols for moving targets of particular shapes and sizes.

A large portion of algorithms within multi-vehicle formation for target tracking are related to formation control to observe a known target, and, therefore, do not require an estimation or circumnavigation. This type of work focuses, for in-

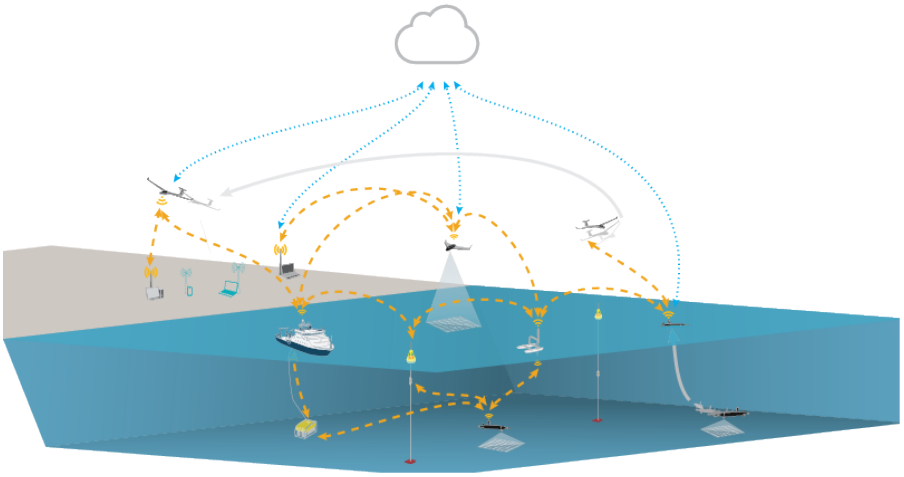

Figure 2.2: Design, construction, and operation of unmanned underwater, surface and air vehicles development of tools and technologies for the deployment of networked vehicle systems. (Courtesy of LSTS [14])

stance, on fast and energy efficient convergence of each vehicle to a desired position while sometimes optimising communication costs. In Fig. 2.3 we can see a classical example of formation control without estimation or circumnavigation. One of the earliest results proposes a path following algorithm for formation control of a multi-agent system [17]. The authors prove that, if the tracking errors are bounded, their method stabilises the formation error. However, it is assumed that there is perfect information available about the path to follow. In [18], a control protocol is designed for avoiding obstacles and inter-agent collisions while converging to a specified target position, and forming an equilateral triangular formation around the target. Also, in [19], [20], and in Section 6.3.1 of [21], formation protocols are proposed where the robots are capable of converging towards a desired pattern by acquiring their distances between each other. Additionally, in [22] and [23], controllers are synthesised for a swarm of agents to generate a desired two-dimensional geometric pattern specified by a simple, closed planar curve. It is assumed that the shape is given to the swarm and is not estimated in real-time. Finally, an example of optimal circle circumnavigation is presented in [24], where the objective is area scanning. Note that, the literature above does not cover target estimation.

There is extensive work on circumnavigation algorithms that integrate formation control with target estimation. A target is generally defined as a moving unit point and the vehicles measure and estimate its location. The algorithms tend to be either distance-based, bearing-based, or both. One of the first work on distance-based algorithms deals with agents moving around the target on a circle while forming an optimal geometry [25]. In [26] there is only one agent and, therefore, no formation

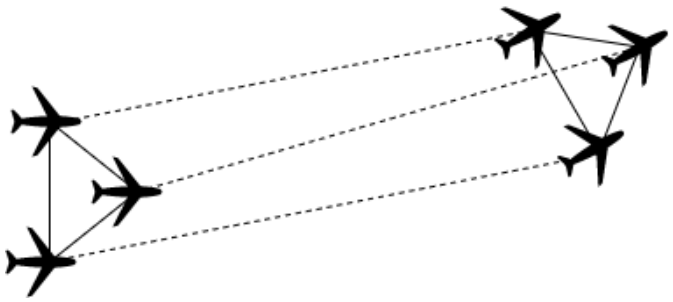

Figure 2.3: Three planes maintain triangular formation while following a path.

control. This agent is capable of measuring its distance to the unit point target and converge to it using sliding mode control. A closely related work [27] proposes an adaptive protocol to circumnavigate around a moving point. The authors employ adaptive estimation for point tracking at a known distance. In [28], a distance-based algorithm for pattern formation is proposed which guarantees convergence while tracking the target. The agents detect their distance to other agents as well as to the moving target and follow it while circumnavigating. [29] devises an algorithm such that one robot can circumnavigate a circular target from a prescribed radius using bearing measurements. Related results [30] and [31] use either bearing or distance measurements to the target while using a network of autonomous agents to circumnavigate. Circumnavigation is done with a predefined distance to the target, which is also the case in [32] where a localization and circumnavigation algorithm of a slowly drifting target is proposed. Here, the authors analyse distance-based and bearing-based measurements as well as various communication protocols. In [33] the agent has access to the bearing measure towards the target. The biggest distinction between these works and the ones we develop in this thesis is the target. In the above articles, the target is assumed to be a unit point and the agents must circumnavigate it at a predetermined relative distance. Whereas our problem deals with a dynamic irregular shape. There is also work on multi-vehicle formation control and target tracking when the target is not a unit point. [34] proposes a protocol for target tracking in 3D with guaranteed collision avoidance. The difference is that, in this paper, it is assumed that the target is a fixed object that may move and rotate but never change its shape, which is different from our case. In the literature above, the authors did not account for a shape shifting target that requires constant measuring and estimation while performing formation control for target circumnavigation.

Chapter 3

Cooperative circumnavigation using adaptive estimation

In this chapter we discuss the problem of multi-vehicle target tracking. This target is an irregular dynamic shape approximated by a circle with moving center and time-varying radius. We will use adaptive estimation while circumnavigating the target with a system of USVs. The multiple USV system is composed of n USVs of which one is equipped with an UAV that is capable of measuring both the distance to the boundary of the target and to its center. This USV equipped with the UAV uses adaptive estimation to calculate the location and size of the mobile target. The USV system must circumnavigate the boundary of the target while forming a regular polygon.

In Section 3.1 we describe the system mathematically and we formulate the problem to be solved in the following section. In Section 3.2 we design two algorithms: One for the adaptive estimation of the target using the UAV's measurements and the other for the control protocol to be applied by all USVs in their navigation. In Section 3.3 the convergence of both algorithms to the desired state is proved up to a limit bound. Finally, in Section 3.4 two simulated examples are provided to verify the performance of the algorithms designed.

3.1 Problem statement

We consider the problem of tracking a shape using a multi-USV system and a UAV. This target shape may be very irregular and with time-varying parameters. We assume the shape is close to a circle. The UAV provides an initial image of the target which confirms such assumption and helps us deploy the USVs.

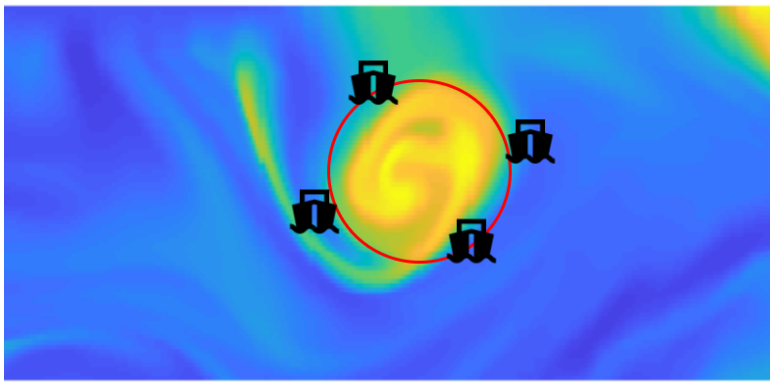

Figure 3.1: 4 USVs circumnavigating a circular algal bloom

3.1.1 System description

We define this circle as

$$(\mathbf{c}, r) \in \mathbb{R}^3, \tag{3.1}$$

where $\mathbf{c} = (x, y)$ and r are the center and the radius of the circle, respectively. We denote $(\hat{\mathbf{c}}, \hat{r}) \in \mathbb{R}^3$ as the estimates of the circle. Then the UAV would provide initial estimates $\hat{\mathbf{c}}(0) = (\hat{x}(0), \hat{y}(0))$ and $\hat{r}(0)$.

This UAV obtains data from the target and shares it with the USVs so they can move towards the target. The UAV constantly measures its distance from the target, calculates its target estimates, and shares it with all USVs. The measurements consist of its distance to the center and to its boundary. Each USV has access to its GPS position and to the GPS position of the USV in front of it, counterclockwise.

The multi-USV system will jointly circumnavigate the target and provide real time information of different fronts. We define n USVs and, using the UAV information, they are initialised at positions $\mathbf{p}_i(0)$, $i \in [1, ..., n]$, which are outside of the shape and form a counterclockwise directed ring on the surface. The kinematic of the USVs is of the form

$$\dot{\mathbf{p}}_i = \mathbf{u_i}, \qquad i \in [1, ..., n], \tag{3.2}$$

where $\mathbf{p}_i$ is a vector that contains the position $\mathbf{p}_i = [x_i, y_i]^\top \in \mathbb{R}^2$ and $\mathbf{u_i} \in \mathbb{R}^2$ is the control input.

In order to avoid the USVs concentrating in some region, in which case they may loose information on other fronts, we would like to space them equally along the defined circle. Therefore, we define the counterclockwise angle between the vector $\mathbf{p}_i - \hat{\mathbf{c}}$ and $\mathbf{p}_{i+1} - \hat{\mathbf{c}}$ as β_i for $i = 1, \ldots, n-1$, and the angle between $\mathbf{p}_n - \hat{\mathbf{c}}$ and $\mathbf{p}_1 - \hat{\mathbf{c}}$ as β_n,

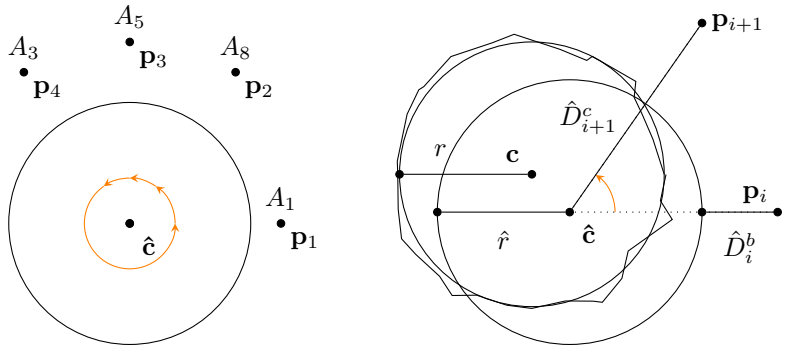

Figure 3.2: (Left) System with vehicles A_1, A_3, A_5, A_8 at positions $\mathbf{p}_1$, $\mathbf{p}_4$, $\mathbf{p}_3$, $\mathbf{p}_2$, respectively. (Right) Estimated $\hat{\mathbf{c}}$, $\hat{r}$, real $\mathbf{c}$, r, and angle β_i between two vehicles at $\mathbf{p}_{i+1}$ and $\mathbf{p}_i$.

$$\begin{aligned} \beta_i &= \angle(\mathbf{p}_{i+1} - \hat{\mathbf{c}}, \mathbf{p}_i - \hat{\mathbf{c}}), \qquad i = 1, \ldots, n-1 \\ \beta_n &= \angle(\mathbf{p}_1 - \hat{\mathbf{c}}, \mathbf{p}_n - \hat{\mathbf{c}}). \end{aligned} \tag{3.3}$$

Then it holds that

$$\beta_i(0) \geq 0, \quad \text{and} \quad \sum_{i=1}^{n} \beta_i(0) = 2\pi. \tag{3.4}$$

This is represented in the left scheme of Fig. 3.2.

Note that the ℓ_2-norm is denoted simply as $\|\cdot\|$ without a subscript. Now we can define the distance from the UAV to the center and the boundary of the target circle as

$$\begin{aligned} D^c_1 &= \|\mathbf{c} - \mathbf{p}_1\| \\ D^b_1 &= |r - D^c_1|, \end{aligned} \tag{3.5}$$

respectively. Note that this UAV senses the distances to the target and then calculates the target estimates. This UAV operation is represented in the left part of Fig. 3.3.

After obtaining the target estimates, each USV i would be able to calculate its own distances $\hat{D}^c_i$ and $\hat{D}^b_i$

$$\begin{aligned} \hat{D}^c_i &= \|\hat{\mathbf{c}} - \mathbf{p}_i\| \\ \hat{D}^b_i &= |\hat{r} - \hat{D}^c_i|, \end{aligned} \tag{3.6}$$

as represented in the right scheme of Fig. 3.2. We summarise each USVs' scheme of computation in the right part of Fig. 3.3.

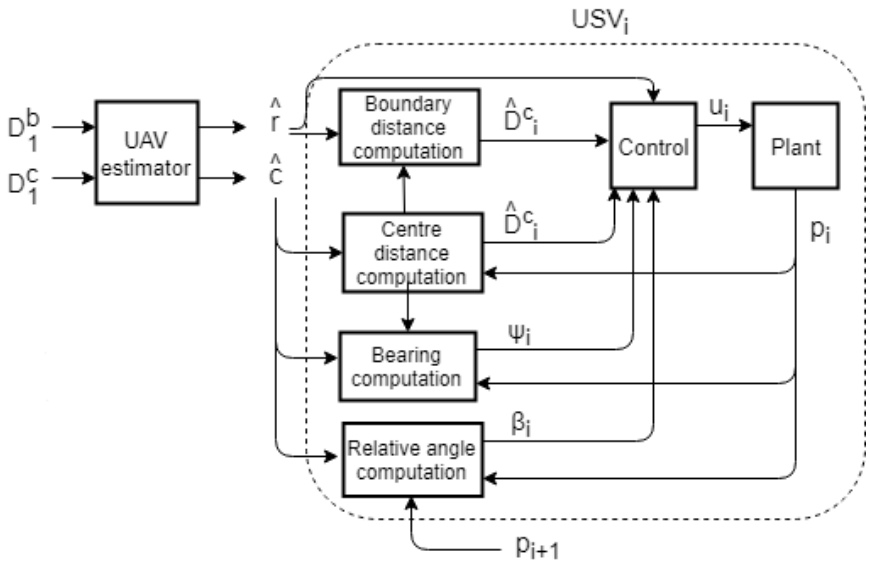

Figure 3.3: The UAV estimates the center and radius of the target based on its distance measurements and shares it with all USVs. Each USV i calculates its control protocol.

3.1.2 Problem formulation

Definition 3.1 (Circumnavigation)**.** *When the target is stationary, i.e.,* $\mathbf{c}$ *and* r *are constant, circumnavigation is achieved if the USVs*

1. *move in a counterclockwise direction on the boundary of the target, and*
2. *are equally distributed along the circle, i.e.,* $\beta_i = \frac{2\pi}{n}$.

More specifically, we say that the circumnavigation is achieved asymptotically if the previous criteria is satisfied for $t \to \infty$.

For the case with time-varying target, we assume that $\|\dot{\mathbf{c}}\| \leq \varepsilon_1$ *and* $|\dot{r}| \leq \varepsilon_2$ *for some positive constant* ε_1 *and* ε_2.

Now we are ready to pose the problem of interest that will be solved in the following sections.

Problem 1. Design a UAV estimator for $\mathbf{c}(t)$ and $r(t)$ when distance measures (3.6) are available to the UAV, and design the control inputs $\mathbf{u}_i$ for the USVs such that for some positive ε_1, ε_2,

$$\|\dot{\mathbf{c}}\| \leq \varepsilon_1, \tag{3.7}$$

$$|\dot{r}| \leq \varepsilon_2, \tag{3.8}$$

there exist positive K_1, K_2, and K_3 satisfying

$$\limsup_{t\to\infty} \|\hat{\mathbf{c}}(t) - \mathbf{c}(t)\| \leq K_1\varepsilon_1, \tag{3.9}$$

$$\limsup_{t\to\infty} |\hat{r}(t) - r(t)| \leq K_2\varepsilon_2, \tag{3.10}$$

$$\limsup_{t\to\infty} |\hat{D}_i^c(t) - \hat{r}(t)| \leq K_3\varepsilon_2, \tag{3.11}$$

$$\lim_{t\to\infty} \beta_i(t) = \frac{2\pi}{n}. \tag{3.12}$$

3.2 Adaptive estimation and control algorithms

In this section, we propose an estimation and control mechanism for Problem 1. We consider n USVs at positions $\mathbf{p}_i$ and one UAV which is capable of measuring its distance D_i^b to the target boundary as well as its distance D_i^c to the target center.

Then, it should estimate $(\mathbf{c}, r)$ from its distance measures, i.e. D_i^b and D_i^c, and share the information with the USVs. Each USV calculates its desired velocity taking into account its angle β_i to the next USV as well as its distance to the target center and boundary, obtained with the estimates of the target.

3.2.1 Adaptive estimation

This subsection relates to the protocol followed by the UAV for estimation. Recalling Fig. 3.3, we will construct the UAV estimator block. Motivated by [27], we propose the following adaptive estimation of the radius r of the target using the UAV A_1 in position $\mathbf{p}_1$. Observe that

$$\frac{d}{dt}(D_1^b)^2 = 2(\dot{r} - \dot{D}_1^c)(r - D_1^c). \tag{3.13}$$

Assume the estimate of r is denoted as $\hat{r}$, we have

$$\frac{1}{2}\big(\frac{d}{dt}(D_1^b)^2 - \frac{d}{dt}(D_1^c)^2\big) + \dot{D}_1^c\hat{r} = \dot{D}_1^c(\hat{r} - r) + \dot{r}(r - D_1^c). \tag{3.14}$$

Then for some positive constant γ the dynamic

$$\dot{\hat{r}} = -\gamma\dot{D}_1^c\big[\frac{1}{2}\big(\frac{d}{dt}(D_1^b)^2 - \frac{d}{dt}(D_1^c)^2\big) + \dot{D}_1^c\hat{r}\big] \tag{3.15}$$

can estimate the variable r under the persistent excitation condition on $\dot{D}_1^c$. Persistent excitation plays a key role in establishing parameter convergence in adaptive identification [35, 36].

Definition 3.2. *(Continuous time persistent excitation condition) [36] The function $f \in \mathcal{L}_e^2(\mathbb{R}^n)$ is said to be* persistently exciting (p.e.) *if there exist positive*

constants ε_1, T *such that for all* $\tau > 0$,

$$\int_{\tau}^{T+\tau} f(t)f(t)^\top dt > \varepsilon_1 I_n.$$

T *will be termed an excitation period of* f.

Then, in this case

$$\frac{d}{dt}(\hat{r} - r) = -\gamma(\dot{D}_1^c)^2(\hat{r} - r) - \vartheta_{\dot{r}}, \tag{3.16}$$

where $\vartheta_{\dot{r}} = \dot{r}(\gamma\dot{D}_1^c(r - D_1^c) + 1)$ is bounded by $M_1\varepsilon_2$. Indeed all its elements are bounded by $M_1 > 0$ and recall that $|\dot{r}| \leq \varepsilon_2$. Note that $r - D_1^c$ is bounded because r and D_1^c are bounded as well. Furthermore, as it will be clear soon, $\vartheta_{\dot{r}}$ can be replaced by $\vartheta_{\dot{r}} = \dot{r}(\gamma V(r - D_1^c) + 1)$ using equations (3.21) and (3.22), where V is the bounded estimate of $\dot{D}_1^c$.

However, the implementation of (3.15) needs the derivative of D_1^b and D_1^c which is not desired. It would require explicit differentiation of measured signals with accompanying noise amplification. Thus, for some positive constant α we adopt the state variable filtering and then design the estimator as follows

$$\dot{z}_1(t) = -\alpha z_1(t) + \frac{1}{2}(D_1^b(t))^2 \tag{3.17}$$

$$\eta(t) = \dot{z}_1(t) \tag{3.18}$$

$$\dot{z}_2(t) = -\alpha z_2(t) + \frac{1}{2}(D_1^c(t))^2 \tag{3.19}$$

$$m(t) = \dot{z}_2(t) \tag{3.20}$$

$$\dot{z}_3(t) = -\alpha z_3(t) + D_1^c(t) \tag{3.21}$$

$$V(t) = \dot{z}_3(t) \tag{3.22}$$

with initial conditions $z_1(0) = z_2(0) = z_3(0) = 0$. Now together the above dynamics, the estimator for r is given as

$$\dot{\hat{r}} = -\gamma V\big[\eta - m + V\hat{r}\big]. \tag{3.23}$$

Now we need are interested in obtaining $\mathbf{c}$ from the measurements D_1^c and D_1^b. Thus, we must use again adaptive estimation for the center $\mathbf{c}$ of the target.

Observe that

$$\frac{d}{dt}(D_1^c)^2 = 2(\dot{\mathbf{p}}_1 - \dot{\mathbf{c}})^\top(\mathbf{p}_1 - \mathbf{c}). \tag{3.24}$$

Assume the estimation of $\mathbf{c}$ is denoted as $\hat{\mathbf{c}}$, we have

$$\frac{1}{2}\big(\frac{d}{dt}(D_1^c)^2 - \frac{d}{dt}\|\mathbf{p}_1\|^2\big) + \dot{\mathbf{p}}_1^\top\hat{\mathbf{c}} = \dot{\mathbf{p}}_1^\top(\hat{\mathbf{c}} - \mathbf{c}) + \dot{\mathbf{c}}^\top(\mathbf{c} - \mathbf{p}_1). \tag{3.25}$$

Then the dynamic

$$\dot{\hat{\mathbf{c}}} = -\gamma \dot{\mathbf{p}}_1 \big[\frac{1}{2}\big(\frac{d}{dt}(D_1^c)^2 - \frac{d}{dt}\|\mathbf{p}_1\|^2\big) + \dot{\mathbf{p}}_1^\top \hat{\mathbf{c}}\big] \tag{3.26}$$

can estimate the parameter $\mathbf{c}$ under some persistent excitation condition on $\dot{\mathbf{p}}_1$. Indeed, in this case

$$\frac{d}{dt}(\hat{\mathbf{c}} - \mathbf{c}) = -\gamma \|\dot{\mathbf{p}}_1\|^2 (\hat{\mathbf{c}} - \mathbf{c}) - \vartheta_{\dot{\mathbf{c}}}, \tag{3.27}$$

where $\vartheta_{\dot{\mathbf{c}}} = \gamma \dot{\mathbf{c}}^\top \dot{\mathbf{p}}_1 (\mathbf{c} - \mathbf{p}_1) + \dot{\mathbf{c}}$ is bounded by $M_2 \varepsilon_1$. Indeed all its elements are bounded by $M_2 > 0$ and recall that $|\dot{\mathbf{c}}| \leq \varepsilon_1$. Note that $\mathbf{c} - \mathbf{p}_1$ is bounded because $\mathbf{c}$ and $\mathbf{p}_1$ are within a finite map. Furthermore, as it will be clear soon, $\vartheta_{\dot{\mathbf{c}}}$ can be replaced by $\vartheta_{\dot{\mathbf{c}}} = \gamma \dot{\mathbf{c}}^\top V_2 (\mathbf{c} - \mathbf{p}_1) + \dot{\mathbf{c}}$ using equations (3.30)-(3.31), where V_2 is the estimate of $\dot{\mathbf{p}}_1$ and it is bounded.

However, the implementation of (3.26) needs the derivative of $\mathbf{p}_1$ and D_1^c which is not desired. Therefore we use the previously defined equation (3.20) for D_1^c and redefine it as $\eta_2(t) = \dot{z}_2(t)$ and add the following filter

$$\dot{z}_4(t) = -\alpha z_4(t) + \frac{1}{2}\mathbf{p}_1(t)\mathbf{p}_1^T(t) \tag{3.28}$$

$$m_2(t) = \dot{z}_4(t) \tag{3.29}$$

$$\dot{z}_5(t) = -\alpha z_5(t) + \mathbf{p}_1(t) \tag{3.30}$$

$$V_2(t) = \dot{z}_5(t) \tag{3.31}$$

with initial conditions $z_4(0) = z_5(0) = 0$. After updating (3.26) with the above dynamics, the estimator for $\mathbf{c}$ is given as

$$\dot{\hat{\mathbf{c}}} = -\gamma V_2 \big[\eta_2 - m_2 + V_2^T \hat{\mathbf{c}}\big]. \tag{3.32}$$

3.2.2 Control algorithm

This subsection relates to the protocol followed by the USVs for control. Recalling Fig. 3.3, we will construct the USV control block. Therefore, we want to obtain the desired control input $\mathbf{u_i}$ using the previously measured and estimated variables.

The total velocity of each USV comprises of two sub-tasks: approaching the target and circumnavigating it. Therefore we define the direction of each USV towards the estimated center of the target as the bearing ψ_i,

$$\psi_{\mathbf{i}} = \frac{\hat{\mathbf{c}} - \mathbf{p}_i}{\hat{D}_i^c} = \frac{\hat{\mathbf{c}} - \mathbf{p}_i}{\|\hat{\mathbf{c}} - \mathbf{p}_i\|}. \tag{3.33}$$

The first sub-task is related to the bearing ψ_i and the second one is related to its perpendicular, $E\psi_i$. We define a rotation matrix E as

$$E = \begin{bmatrix} 0 & 1 \\ -1 & 0 \end{bmatrix}. \tag{3.34}$$

Then, let us first consider the control law $\mathbf{u_i}$ where δ is a parameter to be defined.

$$\mathbf{u_i} = \dot{\hat{\mathbf{c}}} + ((\hat{D}_i^c - \hat{r}) - \frac{1}{\delta}\dot{\hat{r}})\psi_i + \beta_i \hat{D}_i^c E\psi_i. \tag{3.35}$$

The control actuation of a USV is limited, therefore we have to make sure that the implemented control is within the actuation bounds and so we introduce

$$\mathbf{U_i} = \delta \mathbf{u_i} \tag{3.36}$$

where δ is the same as before. For a specific $\mathbf{u_i}$ it is possible to have $\mathbf{U_i}$ within some specified bounds.

3.3 Convergence results

In this section we prove that the estimator and control algorithm proposed in the previous section converge to the desired behaviour.

Theorem 3.1. *The initial condition satisfies $\hat{D}_i^c(0) > \hat{r}(0) > 0$. Suppose $\dot{\mathbf{p}}_1(t)$ and $\dot{D}_1^c(t)$ are p.e., $\|\dot{\mathbf{c}}\| \leq \varepsilon_1$, and $|\dot{r}| \leq \varepsilon_2$. Consider the system (3.35) with the control protocol (3.36), and the initialisation satisfying $\|\mathbf{p}_i(0) - \hat{\mathbf{c}}(0)\| > 0$, then there exists K_1, K_2, and K_3 such that circumnavigation of the moving circle with equally spaced USVs can be achieved asymptotically up to a bounded error, i.e.*

$$\limsup_{t\to\infty} \|\hat{\mathbf{c}}(t) - \mathbf{c}(t)\| \leq K_1\varepsilon_1, \tag{3.37}$$

$$\limsup_{t\to\infty} |\hat{r}(t) - r(t)| \leq K_2\varepsilon_2, \tag{3.38}$$

$$\limsup_{t\to\infty} |\hat{D}_i^c(t) - \hat{r}(t)| \leq K_3\varepsilon_2, \tag{3.39}$$

$$\lim_{t\to\infty} \beta_i(t) = \frac{2\pi}{n}. \tag{3.40}$$

Proof. The proof is divided into four parts. In the first part, we prove that (3.37) and (3.38) hold. In the second part, we prove that the estimated distance $\hat{D}_i^c$ converges to the estimated radius $\hat{r}$, or in other words, that (3.39) holds. In the third part we prove that the singularity of the bearing ψ_i is avoided. In the last part, we show that the angle between the USVs will converge to the average consensus for n USVs, $\beta_i = \frac{2\pi}{n}$, meaning (3.40) holds.

1. Firstly, we prove that (3.37) and (3.38) hold. The proof for boundedness of the center (3.37), can be found on [27], Proposition 7.1. The proof for boundedness of the radius, however, needs to be derived in this paper. Then, we have that

$$\begin{aligned}\dot{\tilde{r}} = \dot{\hat{r}} &= -\gamma V\left[\eta - m + V\hat{r}\right] \\ &= -\gamma V\left[\eta - m + V(\tilde{r} + r)\right] \\ &= -\gamma V^2\tilde{r} - \gamma V\left[\eta - m + Vr\right] \\ &= -\gamma V^2\tilde{r} + G\end{aligned} \tag{3.41}$$

where $G = -\gamma V\big[\eta - m + Vr\big]$. We know that $|G| \leq k_1\epsilon_2$ for some $k_1, \epsilon_2 \geq 0$ because V is bounded and that $|\eta - m + Vr| < k_2$ we can prove that for a Lyapunov function $W_r = \frac{1}{2}\tilde{r}^2$ we get

$$\begin{aligned}\dot{W}_r &= \tilde{r}\dot{\tilde{r}} = \tilde{r}(-\gamma V^2\tilde{r} + G)\\ &= -\gamma V^2\tilde{r}^2 + \tilde{r}G\\ &\leq -\gamma V^2\tilde{r}^2 + k_1\epsilon_2\tilde{r}\end{aligned} \tag{3.42}$$

then we get that for $\dot{W}_r \leq 0$ to hold, $-\gamma V^2\tilde{r}^2 + k_1\epsilon_2\tilde{r} \leq 0$ must hold. So, we have that when $\tilde{r} \geq \frac{k_1\epsilon_2}{\gamma V^2}$ or $\tilde{r} \leq -\frac{k_1\epsilon_2}{\gamma V^2}$, $\dot{W}_r \leq 0$ so that $|\tilde{r}|$ is within $\pm\frac{k_1\epsilon_2}{\gamma V^2}$. This error $\tilde{r}$ is then proved to converge asymptotically to a ball since $\hat{D}_1^c$ is p.e..

2. We prove that all USVs reach the estimate of the boundary of the moving circles asymptotically, i.e., $\lim_{t\to\infty}\|\mathbf{p}_i(t) - \hat{\mathbf{c}}(\mathbf{t})\| = \lim_{t\to\infty}\hat{D}_i^c(t) = \hat{r}(t)$, so (3.39) holds.

   Consider the function $W_i(t) := \hat{D}_i^c(t) - \hat{r}(t)$ whose time derivative for $t \in [0, +\infty)$ is given as

$$\begin{aligned}\dot{W}_i =& \frac{(\hat{\mathbf{c}} - \mathbf{p}_i)^\top(\dot{\hat{\mathbf{c}}} - \dot{\mathbf{p}}_\mathbf{i})}{\hat{D}_i^c} - \dot{\hat{r}}\\ =& -\frac{(\hat{\mathbf{c}} - \mathbf{p}_i)^\top}{\hat{D}_i^c}\delta((\hat{D}_i^c - \hat{r} - \dot{\hat{r}})\psi_i + \beta_i\hat{D}_i^c E\psi_i) - \dot{\hat{r}}\\ =& -\frac{(\hat{\mathbf{c}} - \mathbf{p}_i)^\top}{\hat{D}_i^c}\psi_i\delta(\hat{D}_i^c - \hat{r} - \dot{\hat{r}}) - \frac{(\mathbf{c} - \mathbf{p}_i)^\top}{\hat{D}_i^c}E\psi_i\delta\beta_i\hat{D}_i^c - \dot{\hat{r}}\\ =& -\delta(\hat{D}_i^c - \hat{r} - \dot{\hat{r}}) - \dot{\hat{r}}\\ =& -\delta W_i.\end{aligned}$$

   Hence for $t \in [0, +\infty)$, we have $\hat{D}_i^c(t) = \delta W_i(0)e^{-t} + \hat{r}(t)$ which implies W_i is converging to zero exponentially.

3. Finally, we show that the angle between the USVs will converge to the average consensus for n USVs, $\beta_i = \frac{2\pi}{n}$, so (3.40) holds.

   Firstly, note that we can write an angle between two vectors $\beta_i = \angle(v_2, v_1)$ as

$$\beta_i = 2\,\mathrm{atan2}((v_1 \times v_2)\cdot z, \|v_1\|\|v_2\| + v_1 \cdot v_2) \tag{3.43}$$

   and its derivative as

$$\dot{\beta}_i = \frac{\hat{v_1} \times z}{\|v_1\|}\dot{v_1} - \frac{\hat{v_2} \times z}{\|v_2\|}\dot{v_2} \tag{3.44}$$

   where $z = \frac{v_1 \times v_2}{\|v_1 \times v_2\|}$, $\hat{v_i} = \frac{v_i}{\|v_i\|}$, $i = 1, 2$.

Then, for $v_1 = \mathbf{p}_i - \hat{\mathbf{c}}$ and $v_2 = \mathbf{p}_{i+1} - \hat{\mathbf{c}}$ we get

$$\begin{aligned}
\dot{\beta}_i &= \frac{\hat{v_1} \times z}{\|v_1\|}\dot{v_1} - \frac{\hat{v_2} \times z}{\|v_2\|}\dot{v_2} \\
&= \frac{\hat{v_1} \times z}{\|v_1\|}\delta((\hat{D}_i^c - \hat{r} - \dot{\hat{r}})\psi_i + \beta_i \hat{D}_i^c E\psi_i) \\
&\quad - \frac{\hat{v_2} \times z}{\|v_2\|}\delta((\hat{D}_{i+1}^c - \hat{r} - \dot{\hat{r}})\psi_{i+1} + \beta_{i+1} D_{i+1}^{\hat{c}} E\psi_{i+1}) \\
&= -\frac{1}{\|v_1\|}\beta_i + \frac{1}{\|v_2\|}\beta_{i+1} \\
&= \delta(-\beta_i + \beta_{i+1}), \qquad i = 1, \ldots, n-1 \\
\dot{\beta}_n &= \delta(-\beta_n + \beta_1).
\end{aligned}$$

which can be written in a compact form as following

$$\dot{\beta} = -\delta B^\top \beta \tag{3.45}$$

where B is the incidence matrix of the directed ring graph from v_1 to v_n.

First, we note that the system (3.45) is positive (see e.g., [37]), i.e., $\beta_i(t) \geq 0$ if $\beta_i(0) \geq 0$ for all $t \geq 0$ and $i \in \mathcal{I}$. This proves the positions of the USVs are not interchangeable.

Second, noticing that $B^\top$ is the (in-degree) Laplacian of the directed ring graph which is strongly connected, then by Theorem 6 in [38], β converges to consensus $\frac{2\pi}{n}\mathbb{1}$.

■

Note how the USV A_i will necessarily maintain its relative position $\mathbf{p}_i$ throughout the circumnavigation mission. In fact, this proves that USV A_i is always in position $\mathbf{p}_i$. We proved both convergence of the angle to the average consensus for n USVs and convergence of these vehicles towards the boundary of the target up to a given bound. Therefore, we guarantee collision avoidance.

Recall Definition 1 on persistent excitation. This means that for the persistently exciting condition to apply, the AUV must move in a trajectory that is not confined to a straight line in the 2D space. As referred in [27], the AUV cannot simply head straight towards the target but must execute a richer class of motion..

Note that the p.e. condition is assumed for Theorem 1. and not proved. However, in the results section we will verify if the p.e. assumptions are true for our simulations, within the simulation time.

3.4 Numerical results

In this section, we present simulations for the protocol designed in section 3.3. We use the derived method for estimation of the target (3.23) and (3.32) and

the controlling protocol for the USVs (3.36). For this section, we discretize the whole algorithm to be able to use it computationally. The first subsection takes into account the persistent excitation condition and the second subsection analyses what happens when this condition is not verified.

3.4.1 Simulations with p.e. guarantees

In this subsection, we simulate a moving target with initial position $(x[0], y[0]) = (25, 25)$, radius $r[0] = 10$, and dynamic according to

$$\begin{aligned} x[t+1] &= x[t] + \alpha_1[t] + 0.5 \\ y[t+1] &= y[t] + \alpha_2[t] + 0.5 \\ r[t+1] &= r[t] + \alpha_3[t] \end{aligned} \tag{3.46}$$

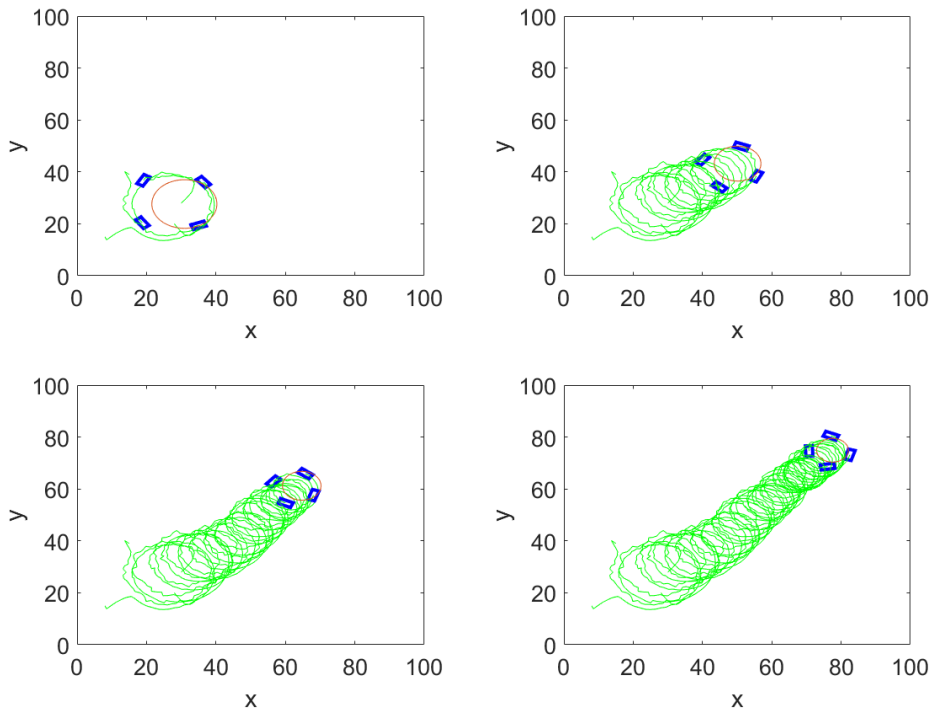

Figure 3.4: Time-lapse of four USVs (blue rectangles) circumnavigating a moving target (red) with representation of their paths (green)

However, we simulate that the UAV will provide as an initial noisy estimate of $(\hat{x}[0], \hat{y}[0]) = (25, 25)$, radius $\hat{r}[0] = 20$. Note that at time $t = 0$ the radius estimate is double the real radius. Here, $\alpha_i[t]$ is a random scalar drawn from the uniform

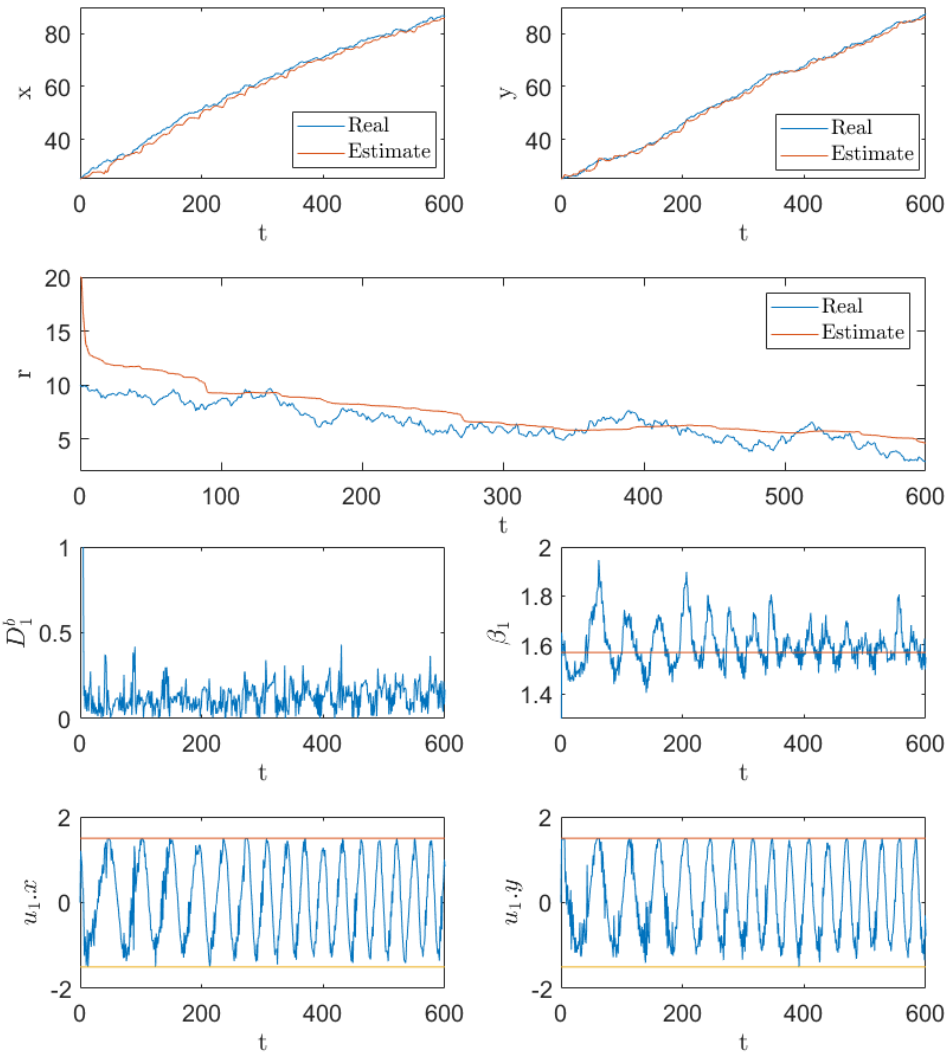

Figure 3.5: First and second row: real and estimated target's center $\mathbf{c} : x, y$ and radius r. Third row: tracking error of USV A_1, D_1^b and angle β_1. Fourth row: control input of USV A_1, $\mathbf{u_1} : x, y$

distribution within the interval of $[-0.5, 0.5]$ for $i = 1, 2, 3$. For this generated target we got the following results. We can see the USVs circumnavigating the moving target in Fig. 3.4. This gives us a more practical idea of how the USVs behave in their target-tracking mission.

Fig. 3.5 shows various plots that analyse the system's behaviour. On the first and second row we compare the real and estimated target. Note that the estimate of the center $\hat{\mathbf{c}}(\hat{x}, \hat{y})$ has an estimation error of up to 2 units. Also note that the estimate of the radius $\hat{r}$ is composed of two instances. In the first, the initial estimate provided by the UAV was very noisy and so we can see the estimate converging rapidly to a more accurate estimation. In the second we can see an estimation error of up to 2 units. On the third row left column, we can see the distance D_i^b of each target to the boundary of the target - the perfect tracking would result in a distance D_i^b of 0 for all USVs, for every time step. Here we have an error of up to 0.5 units, except for the very beginning where the error can reach 10 units. This is merely because in the beginning the USVs are far away from the target.

On the third row right column, we have the angle between USV A_1 and A_2, β_1. Having 4 USVs, the perfect tracking would result in $2\pi/4 = \pi/2 \approx 1.57$ for all USVs, for every time step. We can see this reference as the red line in the plot so we see that, for USV A1, the error is up to 0.2 radians. Finally, on the fourth row we have the control input $\mathbf{u_1}$ of USV A_1, with both parameters x and y. Recall Remark. 2 where we stated that, for a practical implementation, there should be a maximum velocity u_{max}. For this case study we defined that $u_{max} = 1.5$ and we plotted this limit in red. Note how the control input stays within the limit values 1.5 and -1.5.

Since we considered as an assumption that $\dot{\mathbf{p}}_1[t]$ and $\dot{D}_1^c[t]$ are p.e., we now evaluate whether this is actually the case for this simulation example. According to [39], we can adapt Definition 3.2. to the discrete time case so we obtain the functions

$$\begin{aligned} f_{\dot{\mathbf{p}}_1}[t] &= \sum_{k=t}^{t+m} \dot{\mathbf{p}}_1^\top[k]\dot{\mathbf{p}}_1[k], \\ f_{\dot{D}_1^c}[t] &= \sum_{k=t}^{t+m} \dot{D}_1^c[k]^2, \end{aligned} \tag{3.47}$$

which must fulfil $\rho_2 > f_{\dot{\mathbf{p}}_1}[t] > \rho_1$ and $\rho_4 > f_{\dot{D}_1^c}[t] > \rho_3$ for positive ρ_i.

As seen in Fig. 3.6., these conditions are fulfilled for $\rho_1 = 1.1026$, $\rho_2 = 6.8371$, $\rho_3 = 0.2443$, and $\rho_4 = 8.8497$. Then, for these results in this simulating time span, the p.e. conditions hold.

3.4.2 Simulations without p.e. guarantees

In this subsection, we simulate a static target with position $(x[0], y[0]) = (25, 25)$ and radius $r[0] = 10$ for all time t. As in the previous subsection, we simulate that the UAV provides an estimate of $(\hat{x}[0], \hat{y}[0]) = (25, 25)$ and radius $\hat{r}[0] = 20$.

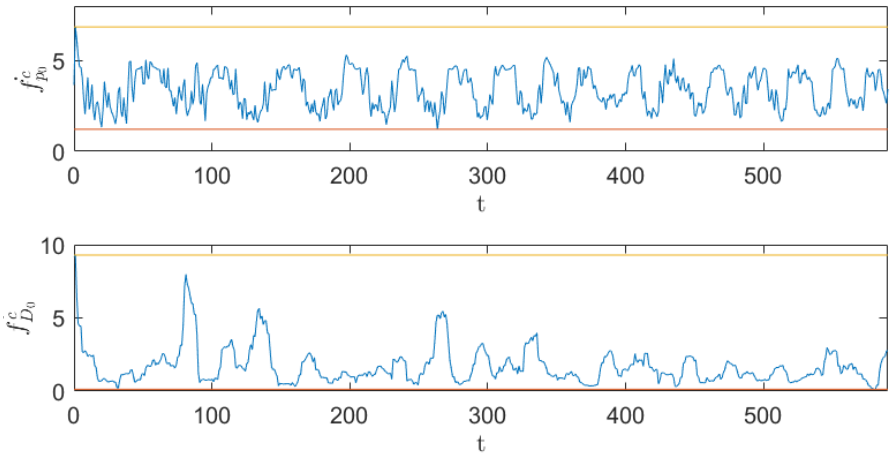

Figure 3.6: First row: $f_{\dot{\mathbf{P}}_1}[t]$ is bounded by strictly positive bounds. Second row: $f_{\dot{D}_1^c}[t]$ is bounded by strictly positive bounds.

This means that the estimates for the center will not have any initial error and the estimate for the radius will have an error of $e_r[0] = \hat{r}[0] - r[0] = 20 - 10 = 10$.

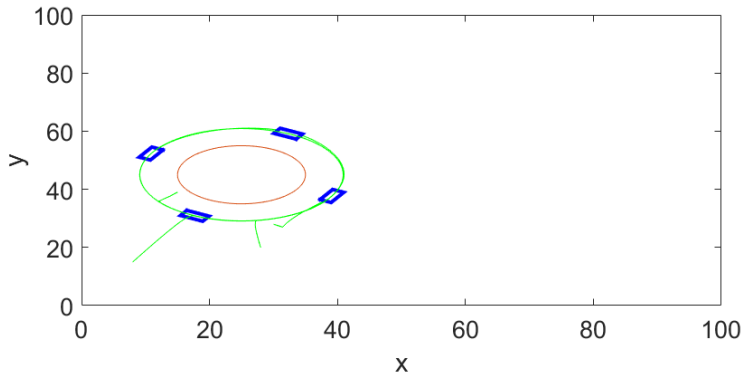

Figure 3.7: Four USVs (blue rectangles) circumnavigating a moving target (red) with representation of their paths (green).

As seen in Fig. 3.7, the estimation of the position seems correct but the estimation of the radius seems wrong.

From the first row Fig. 3.8 we can see how the estimates for the center $\mathbf{c}(x, y)$ are correct for all the simulation time. However, from the second row we can see a steady state error for the estimation of r. Recall that the estimators derived in 3.3

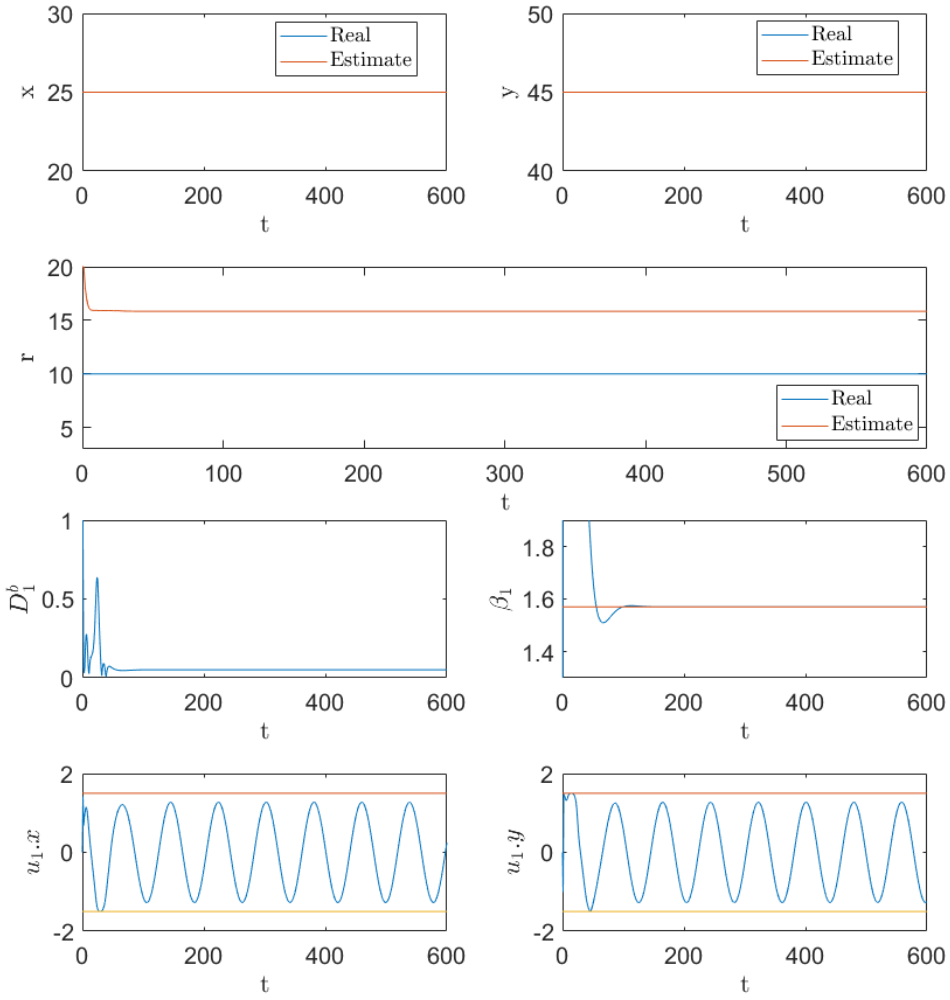

Figure 3.8: First and second row: real and estimated target's center $\mathbf{c} : x, y$ and radius r. Third row: tracking error of USV A_1, D_1^b and angle β_1. Fourth row: control input of USV A_1, $\mathbf{u_1} : x, y$

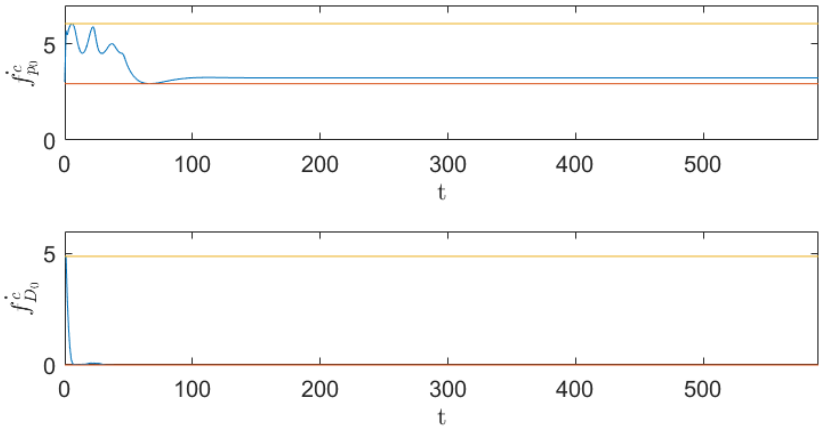

Figure 3.9: First row: $f_{\dot{\mathbf{p}}_1}(t)$ is bounded by strictly positive bounds. Second row: $f_{\dot{D}_1^c}(t)$ is bounded by a strictly positive bound and zero.

for $\mathbf{c}$ and r rely on the p.e. conditions for $\dot{\mathbf{p}}_1$ and $\dot{D}_1^c$, respectively. Then, it seems that the p.e. condition on $\dot{D}_1^c$ does not hold, and, therefore, the estimation of r does not convergence to the real r.

From Fig. 3.9 we can conclude that, for this simulation time, even though the p.e. condition is verified for $\dot{\mathbf{p}}_1$, it is not verified for D_1^c since for some time t the minimum bound is not strictly positive.

3.5 Summary

In this chapter we considered the problem of multi-vehicle target tracking. We assumed that the target was an irregular dynamic shape approximated by a circle with moving center and varying radius. We defined the problem mathematically by introducing relevant variables and equations that relate them. We also defined the measurements available to each agent as well as the estimation and circumnavigation objectives. We created an adaptive estimation algorithm as well as a control algorithm and we proved their mathematical convergence up to a bound according to our objectives. We presented two simulation results: one to analyse convergence performance and the other to represent the need for persistence of excitation when applying the developed algorithms.

Chapter 4

Cooperative circumnavigation with distributed sensing

In this chapter we define a different setup than in Chapter 3 and, therefore, a different algorithm to solve the multi-vehicle target tracking problem. We try to decentralise the measurement step by having all vehicles capable of collecting data and sharing this data to achieve target estimation. As in the previous chapter, we consider that the target is an irregular dynamic shape approximated by a circle with moving center and varying radius. In this chapter, the USV system is composed of n USVs, all measuring their distance to the boundary of the target. The USV system must circumnavigate the boundary of the target while forming a regular polygon.

In Section 4.1 we describe the system mathematically and we formulate the problem to be solved in the following section. In Section 4.2 we design two algorithms: one for finding the optimal circle target using the UAV's measurements and another for the control protocol to be applied by all USVs in their navigation. In Section 4.3 the convergence of both algorithms to the desired state is proved up to a limit bound. Finally, in Section 4.4 a simulated example using SINMOD data is provided to verify the performance of the algorithms designed.

4.1 Problem statement

We consider the problem of tracking a circular shape using a multi-robot system and a satellite. This shape may be very irregular and unstable over time. We assume the shape can be approximated by a circle. An initial image of the algal bloom confirms such assumption, as seen in Fig. 4.1, and then we can decide to use our algorithm to deploy the agents.

We define this circle as

$$(\mathbf{c}, r) \in \mathbb{R}^3, \tag{4.1}$$

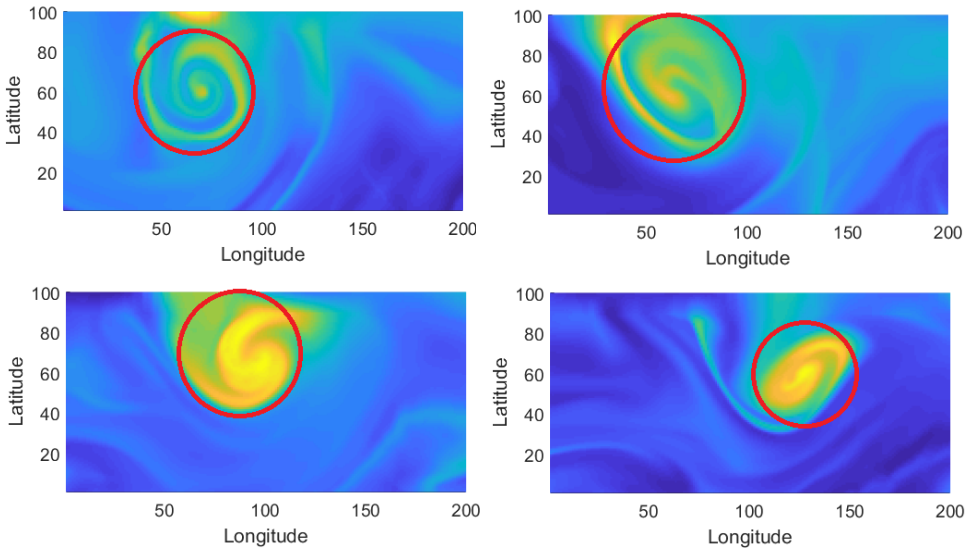

Figure 4.1: Time-lapse of the algal bloom progression. There is approximately half a day between each image. Warm colours (yellow, orange, green) indicate high density of algal and cold colours (blues) indicate low density of algal.

where $\mathbf{c} = (x, y)$ and r are the center and the radius of the circle, respectively. After confirming the algal bloom is close enough to a circle we can then estimate it by our robot's measurements. This estimate is represented as $(\hat{\mathbf{c}}, \hat{r}) \in \mathbb{R}^3$. Note that the usage of a circle shape does not compromise the generality of the algorithm. Instead, it guarantees a smooth circumnavigation for any irregular shape close to a circle. Similar algorithm can be done for shapes that can be approximated by ellipsoids, but we present a simpler case, namely with circle shapes, for notation simplicity.

In order to solve this tracking problem we use two types of tools: a satellite and a system of robots. The satellite obtains data from the target in the form an image depending on the weather. Then, it calculates by image processing the possible initial center and radius of such circle and shares it with the robots so they can move towards the target and initiate circumnavigation. So, the satellite would provide initial estimates $\hat{\mathbf{c}}(0) = (\hat{x}(0), \hat{y}(0))$ and $\hat{r}(0)$. The robots constantly measure their distances to the target's boundary, as well as whether they're inside or outside the target, and share it with the other robots. Each robot has access to its GPS position and to the position of the robot in front of it. This communication scheme is represented in Fig. 4.2. Values such as β_i, $\mathbf{p}_i$, and D_i^b will be soon properly defined.

The system of robots will jointly circumnavigate the target and provide real

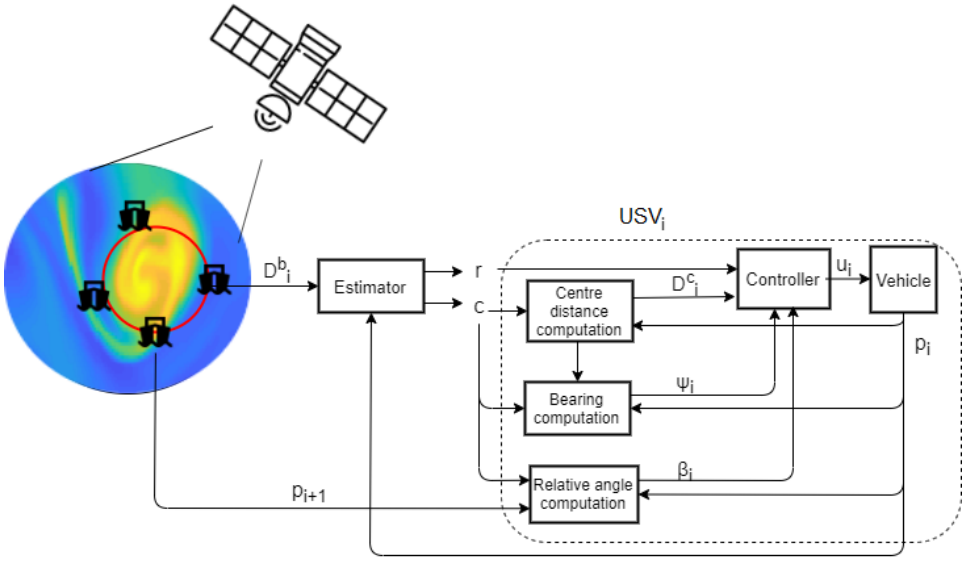

Figure 4.2: Each USV estimates the center and radius of the target based on its distance measurements and shares it with all USVs. Each USV i calculates its control protocol.

time information of different fronts. We define we have n agents and, using the satellite information, they are initialised at positions $\mathbf{p}_i(0)$, $i \in [1, \dots, n]$, which are outside of the shape and form a counterclockwise directed ring on the surface. The kinematic of the agents is of the form

$$\dot{\mathbf{p}}_i = \mathbf{u_i}, \qquad i \in [1, \dots, n], \tag{4.2}$$

where $\mathbf{p}_i$ is a vector that contains the position $\mathbf{p}_i = [x_i, y_i]^\top \in \mathbb{R}^2$ and $\mathbf{u_i} \in \mathbb{R}^2$ is the control input.

In order to avoid the agents concentrating in some region, in which case they may loose information on other fronts, we would like to space the agents equally along the defined circle. Therefore, we introduce two more parameters. The counterclockwise angle between the vector $\mathbf{p}_i - \hat{\mathbf{c}}$ and $\mathbf{p}_{i+1} - \hat{\mathbf{c}}$ is denoted as β_i for $i = 1, \dots, n-1$, and the angle between $\mathbf{p}_n - \hat{\mathbf{c}}$ and $\mathbf{p}_1 - \hat{\mathbf{c}}$ is denoted as β_n, i.e.,

$$\begin{aligned} \beta_i &= \angle(\mathbf{p}_{i+1} - \hat{\mathbf{c}}, \mathbf{p}_i - \hat{\mathbf{c}}), \qquad i = 1, \dots, n-1 \\ \beta_n &= \angle(\mathbf{p}_1 - \hat{\mathbf{c}}, \mathbf{p}_n - \hat{\mathbf{c}}). \end{aligned} \tag{4.3}$$

Notice that in this case,

$$\beta_i(0) \geq 0, \quad \text{and} \quad \sum_{i=1}^{n} \beta_i(0) = 2\pi. \tag{4.4}$$

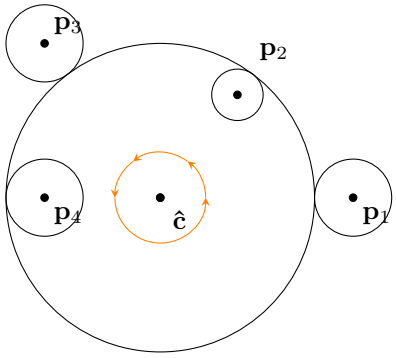

Figure 4.3: Example scheme of the system with four agents at positions p_1, p_4, p_3, p_2. Note how each of them has access to the distance to the boundary, which represented by a circumference.

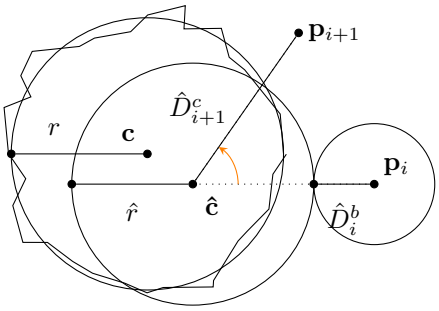

Figure 4.4: Scheme of the estimated $\hat{\mathbf{c}}$, $\hat{r}$ and the real target $\mathbf{c}$, r as well as the angle β_i between two agents at $\mathbf{p}_{i+1}$ and $\mathbf{p}_i$

This is represented in figure Fig. 4.3.

We can define the distance of each agent i to the center as $D_i^c = \|\mathbf{c} - \mathbf{p}_i\|$. Since we do not have access to the center $\mathbf{c}$, the distance to the estimated center is represented as $\hat{D}_i^c = \|\hat{\mathbf{c}} - \mathbf{p}_i\|$. Then, knowing that each robot has access to its distance to the boundary, we can define it as

$$D_i^b = D_i^c - r. \tag{4.5}$$

This value is constantly measured by each agent, as in Fig. 4.3 and Fig. 4.4. Note that D_i^b is positive if the agent is outside the algal bloom area or negative if it is inside the algal bloom area. For example, if an agent i is inside of the circle about 5 meters then $D_i^b = -5$ and if this agent is outside of the circle about 5 meters then $D_i^b = 5$.

Now we are ready to pose the problem of interest that will be solved in the following sections.

Problem 2. Design estimators for $\mathbf{c}(t)$ and $r(t)$ when both the distance measures (4.5) and GPS positions are available to each agent. Design the control input $\mathbf{u}_i$ for all the agents such that for some positive ε_1, ε_2,

$$\|\dot{\hat{\mathbf{c}}}\| \leq \varepsilon_1 \tag{4.6}$$
$$|\dot{\hat{r}}| \leq \varepsilon_2, \tag{4.7}$$

there exist positive K_1, K_2, and K_3 satisfying

$$\limsup_{t\to\infty} \|\hat{\mathbf{c}}(t) - \mathbf{c}(t)\| \leq K_1\varepsilon_1, \tag{4.8}$$
$$\limsup_{t\to\infty} |\hat{r}(t) - r(t)| \leq K_2\varepsilon_2, \tag{4.9}$$
$$\limsup_{t\to\infty} |D_i^b(t)| \leq K_3\varepsilon_2, \tag{4.10}$$
$$\lim_{t\to\infty} \beta_i(t) = \frac{2\pi}{n}. \tag{4.11}$$

4.2 Optimal circle estimation and control algorithms

Here follows our solution for Problem 2. We consider n agents with positions $\mathbf{p}_i$ and we assume all of them are capable of measuring their distances D_i^b to the target boundary including whether they're inside (D_i^b is negative) or outside (D_i^b is positive) of it. Then, they should estimate $(\mathbf{c}, r)$ from their shared measurements. For robustness, they update their estimates by taking the average of the estimated variables by the n agents. Also, if one or more agents suffered faulty measurements due to bad conditions or failure, the system is ready to support that situation by using the remaining agent's estimates. Each agent calculates its desired velocity taking into account its angle β_i to the next agent and its distance to the boundary. The scheme on Fig. 4.5 summarises this algorithm loop.

First step is the estimation of the circle. Having all the agents constantly measuring D_i^b we can fit a unique circle as in Fig. 4.3, given that the target shape is a circle. Mathematically, such circle can be obtained through triangulation and, therefore, we would only need 3 agents to obtain a unique solution. However, for better coverage of all the fronts and for robustness, more than 3 agents are considered. Note that, in this paper's result section we used 4 agents. So, we apply the least squares method to obtain the approximated circle as in (4.12).

$$\min_{\hat{\mathbf{c}},\hat{r}} \sum_{i}^{n} \left(\|\mathbf{p}_i - \hat{\mathbf{c}}\| - (\hat{r} + D_i^b)\right)^2. \tag{4.12}$$
$$s.t \qquad \hat{r} > 0.$$

Now, we want to obtain the desired control input $\mathbf{u_i}$ using the previously measured and estimated variables. The total velocity of each agent comprises of two

sub-tasks: approaching the target and circumnavigating it. Therefore we define the direction of each agents towards the center of the target as the bearing $\psi_{\mathbf{i}}(t)$,

$$\psi_i = \frac{\hat{\mathbf{c}} - \mathbf{p}_i}{\hat{D}_i^c} = \frac{\hat{\mathbf{c}} - \mathbf{p}_i}{\|\hat{\mathbf{c}} - \mathbf{p}_i\|}. \tag{4.13}$$

Note that $\psi_{\mathbf{i}}$ in (4.13) is not well-defined when $\hat{D}_i^c = 0$, thus we need to prove that this singularity is avoided for all $t \geq 0$ in Theorem 4.1.

In order to build the control, we need to define $\dot{\hat{\mathbf{c}}}$ and $\dot{\hat{r}}$. Even though $\mathbf{c}(t)$ and $r(t)$ are continuous functions, our estimates $\dot{\hat{\mathbf{c}}}$ and $\dot{\hat{r}}$ are, inevitably, a discrete function. Therefore, for each time interval Δ_T, we approximate $\dot{\hat{\mathbf{c}}}(t)$ and $\dot{\hat{r}}(t)$ as

$$\dot{\hat{\mathbf{c}}}[t] = \frac{\hat{\mathbf{c}}(t + \Delta_T) - \hat{\mathbf{c}}[t]}{\Delta_T} \tag{4.14}$$

$$\dot{\hat{r}}[t] = \frac{\hat{r}(t + \Delta_T) - \hat{r}[t]}{\Delta_T} \tag{4.15}$$

The first sub-task is related to the bearing ψ_i and the second one is related to its perpendicular, $E\psi_i$. Therefore, let us first consider the control law $\mathbf{u_i}$ where δ is a parameter to be defined.

$$\mathbf{u_i} = \dot{\hat{\mathbf{c}}} + ((\hat{D}_i^c - \hat{r}) - \frac{1}{\delta}\dot{\hat{r}})\psi_i + \beta_i \hat{D}_i^c E\psi_i \tag{4.16}$$

The control actuation of a USV is limited, therefore we have to make sure that the implemented control is within the actuation bounds and so we introduce

$$\mathbf{U_i} = \delta \mathbf{u_i} \tag{4.17}$$

where δ is the same as before. For a specific $\mathbf{u_i}$ it is possible to have $\mathbf{U_i}$ within some specified bounds.

4.3 Convergence results

Theorem 4.1. *Consider the system* (4.2) *with the control protocol* (4.17)*, and* $\|\dot{\mathbf{c}}\| \leq \varepsilon_1$*,* $|\dot{r}| \leq \varepsilon_2$*, then there exists* K_1*,* K_2*, and* K_3 *such that circumnavigation of the moving circle with equally spaced agents can be achieved asymptotically up to a bounded error, i.e.*

$$\limsup_{t\to\infty} \|\hat{\mathbf{c}}(t) - \mathbf{c}(t)\| \leq K_1\varepsilon_1, \tag{4.18}$$

$$\limsup_{t\to\infty} |\hat{r}(t) - r(t)| \leq K_2\varepsilon_2, \tag{4.19}$$

$$\limsup_{t\to\infty} |D_i^b(t)| \leq K_3\varepsilon_2, \tag{4.20}$$

$$\lim_{t\to\infty} \beta_i(t) = \frac{2\pi}{n}. \tag{4.21}$$

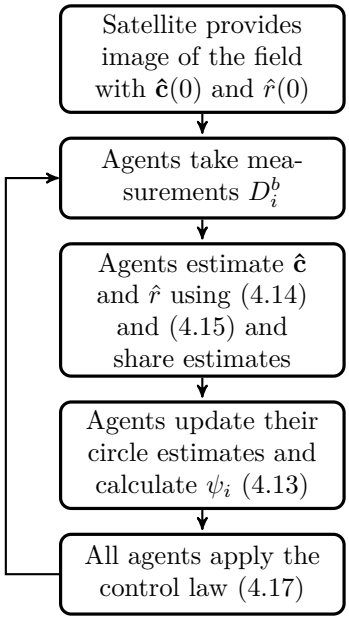

Figure 4.5: Scheme of the algorithm run on the system

Proof. The proof is divided into three parts. In the first part, we prove that the estimated distance $\hat{D}_i^c$ converges to the estimated radius $\hat{r}$, or in other words, that (4.20) holds. In the second part we prove that the singularity of the bearing ψ_i is avoided. In the last part, we show that the angle between the agents will converge to the average consensus for n agents, $\beta_i = \frac{2\pi}{n}$, meaning (4.21) holds.

1. We prove that all agents reach the estimate of the boundary of the moving circles asymptotically, i.e., $\lim_{t\to\infty} \hat{D}_i^c(t) = \hat{r}(t)$, so (4.20) holds.

   Consider the function $W_i(t) := \hat{D}_i^c(t) - \hat{r}(t)$ whose time derivative for $t \in [0, \tau_{\max})$ is given as

$$\begin{aligned}
\dot{W}_i =& \frac{(\hat{\mathbf{c}} - \mathbf{p}_i)^\top (\dot{\hat{\mathbf{c}}} - \dot{\mathbf{p}}_i)}{\hat{D}_i^c} - \dot{\hat{r}} \\
=& -\frac{(\hat{\mathbf{c}} - \mathbf{p}_i)^\top}{\hat{D}_i^c} \psi_i \delta (\hat{D}_i^c - \hat{r} - \dot{\hat{r}}) - \frac{(\mathbf{c} - \mathbf{p}_i)^\top}{\hat{D}_i^c} E \psi_i \delta \beta_i \hat{D}_i^c - \dot{\hat{r}} \\
=& -\delta (\hat{D}_i^c - \hat{r} - \dot{\hat{r}}) - \dot{\hat{r}} \\
=& -\delta W_i.
\end{aligned}$$

   Hence for $t \in [0, +\infty)$, we have $\hat{D}_i^c(t) = \delta W_i(0) e^{-t} + \hat{r}(t)$ which implies W_i is converging to zero exponentially.

2. Now, we prove that ψ_i in (4.13) is well-defined, or in other words, that its singularity is avoided for all time $t \geq 0$, $\hat{D}_i^c \neq 0 \ \forall t$.

   Having $\hat{D}_i^c(t) = \delta W_i(0)e^{-t} + \hat{r}(t)$ from the previous proof and knowing that $W_i(0)$ is always positive and that it converges to zero exponentially, we have that if $\hat{r}(t) > 0$ then $\hat{D}_i^c(t) > 0$, $\forall t$.

   So we would have to prove that $\hat{r}(t) > 0 \ \forall t$. Given that we use the least squares method to obtain the estimate of the radius, we can see how one of the constraints guarantees that $\hat{r}(t) > 0 \ \forall t$. Then we conclude that $\hat{D}_i^c \neq 0$ $\forall t$ and that the bearing $\psi_i(t)$ is well defined $\forall t$.

3. Finally, we show that the angle between the agents will converge to the average consensus for n agents, $\beta_i = \frac{2\pi}{n}$, so (4.21) holds.

   Firstly, note that we can write an angle between two vectors $\beta_i = \angle(v_2, v_1)$ as

   $$\beta_i = 2\,\mathrm{atan2}((v_1 \times v_2) \cdot z, \|v_1\|\|v_2\| + v_1 \cdot v_2) \tag{4.22}$$

   and its derivative as

   $$\dot{\beta}_i = \frac{\hat{v_1} \times z}{\|v_1\|}\dot{v_1} - \frac{\hat{v_2} \times z}{\|v_2\|}\dot{v_2} \tag{4.23}$$

   where $z = \frac{v_1 \times v_2}{\|v_1 \times v_2\|}, \hat{v_i} = \frac{v_i}{\|v_i\|}, i = 1, 2.$

   Then, for $v_1 = \mathbf{p}_i - \hat{\mathbf{c}}$ and $v_2 = \mathbf{p}_{i+1} - \hat{\mathbf{c}}$ we get

   $$\begin{aligned}
   \dot{\beta}_i &= \frac{\hat{v_1} \times z}{\|v_1\|}\dot{v_1} - \frac{\hat{v_2} \times z}{\|v_2\|}\dot{v_2} \\
   &= \frac{\hat{v_1} \times z}{\|v_1\|}\delta((\hat{D}_i^c - \hat{r} - \dot{\hat{r}})\psi_i + \beta_i \hat{D}_i^c E\psi_i) \\
   &\quad - \frac{\hat{v_2} \times z}{\|v_2\|}\delta((\hat{D}_{i+1}^c - \hat{r} - \dot{\hat{r}})\psi_{i+1} + \beta_{i+1} D_{i+1}^{\hat{c}} E\psi_{i+1}) \\
   &= -\frac{1}{\|v_1\|}\beta_i + \frac{1}{\|v_2\|}\beta_{i+1} \\
   &= \delta(-\beta_i + \beta_{i+1}), \qquad i = 1, \ldots, n-1 \\
   \dot{\beta}_n &= \delta(-\beta_n + \beta_1).
   \end{aligned}$$

   which can be written in a compact form as following

   $$\dot{\beta} = -\delta B^\top \beta \tag{4.24}$$

   where B is the incidence matrix of the directed ring graph from v_1 to v_n.

   First, we note that the system (4.24) is positive (see e.g., [37]), i.e., $\beta_i(t) \geq 0$ if $\beta_i(0) \geq 0$ for all $t \geq 0$ and $i \in \mathcal{I}$. This proves the positions of the agents are not interchangeable. Second, noticing that $B^\top$ is the (in-degree) Laplacian of the directed ring graph which is strongly connected, then by Theorem 6 in [38], β converges to consensus $\frac{2\pi}{n}\mathbb{1}$. ■

Remark 1. *Note how the agent A_i will necessarily maintain its relative position p_i throughout the circumnavigation mission. In fact, we can prove that agent A_i is always in position p_i.*

Remark 2. *We proved both convergence of the angle to the average consensus for n agents and convergence of these agents towards the boundary of the target up to a given bound. Therefore, we guarantee collision avoidance.*

4.4 Simulation results

In this section, we present simulations for the protocol designed in section 4.2. We use the derived method for estimation of the target (4.12) and the controlling protocol for the agents (4.17). For this section, we discretize the whole algorithm to be able to use it computationally.

We use the target present in the images provided by SINMOD simulations [40]. The present simulation corresponds to approximately 4 days of data and the target we obtained is approximately 1-3km in radius.

In Fig. 4.6 we can see the robot system circumnavigating the algal bloom target in a time-lapse. This specific algal bloom target is quite a challenge as it shape shifts quite abruptly. Note that the agents were deployed in positions in the boundary so their initial error $D_i^b(0)$ is zero. Note also how, in some instances of the mission, the target moves fast to such extent that the robots present a delay. This effect is foreseen and explained in Theorem 4.1.

Analysing the simulations, we observe each variable in Fig. 4.7. Firstly, we can see the comparison between the real position of the target and the estimates our algorithm provided. We can observe that the estimation follows closely the real value with an apparently very small error. Secondly, we analyse the distance of agent 1 to the boundary D_1^b and the angle between agent 1 and 2, β_1. We can see the error is within the expected boundaries according to Theorem 1. Regarding the distance to the boundary, the error never exceeds 2 units (200 meters) and is most of the time up to 1 unit (100 meters). Note that each x and y coordinate unit corresponds to about 100 meters. Also, each time iteration unit corresponds to 6min. As for the angle between agents the maximum error is 0.2 radians which corresponds to a maximum angle error of 11 degrees. If we look at the plots for the control input of our agents, namely, for agent 1, we can see how the control was applied up to a maximum value. We defined the maximum speed of the agent for each coordinate to be 2 y units per 1 x unit which corresponds to 2km/h in each Cartesian direction (200m / 6min = 2km/h).

Having the same protocols and data set, we simulated a different scenario in which a fifth vehicle enters the system as seen in Fig. 4.8. We can see how the vehicles adjust the angles between each other to make space for the new vehicle. Notice how, on the last figure, the vehicles seem to be converging to a regular polygon formation. This scenario represents the scaling possibility of our protocol.

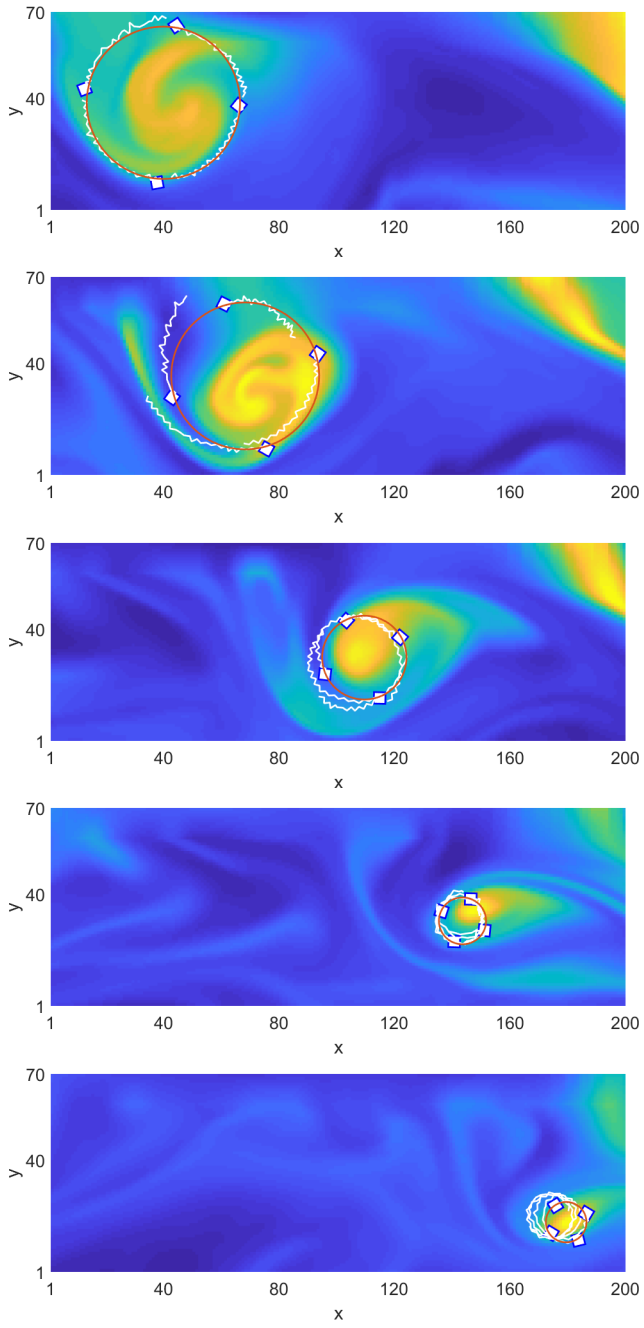

Figure 4.6: Time-lapse of four agents circumnavigating a moving target (red) with representation of their paths (white). Each plot is approximately half a day after the previous.

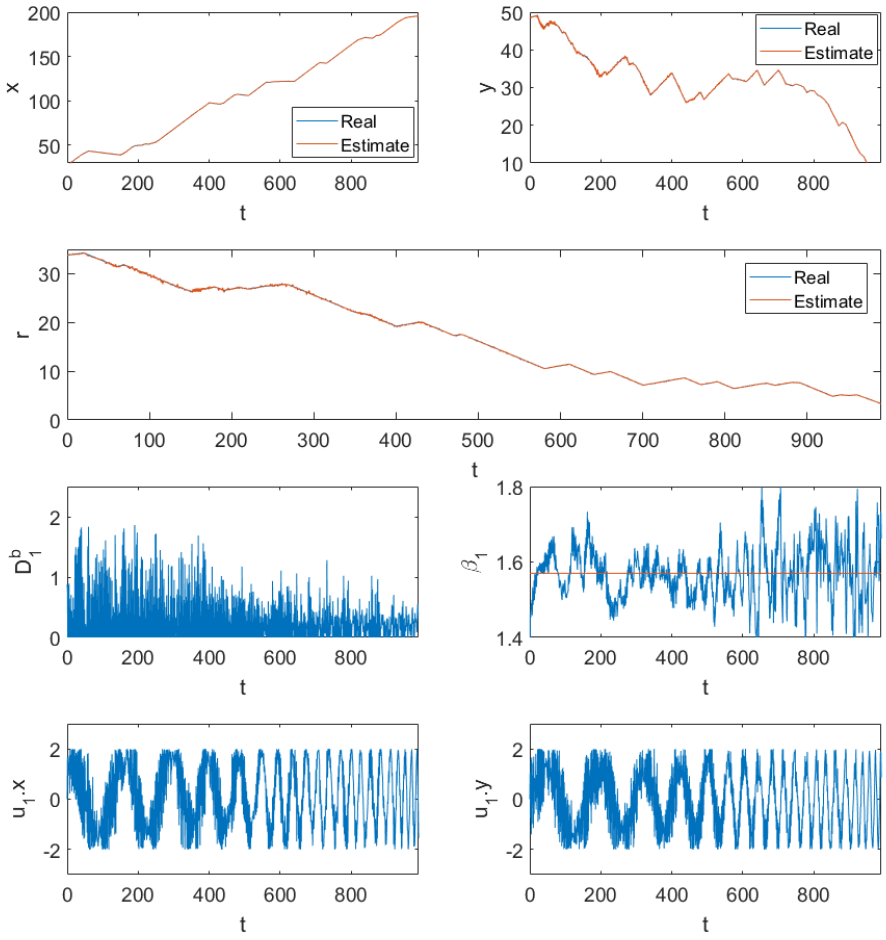

Figure 4.7: First and second row: real and estimated target's center $\mathbf{c} : x, y$ and radius r. Third row: tracking error of agent 1, D_1^b and angle β_1. Fourth row: control input of agent 1, $\mathbf{u_1} : x, y$

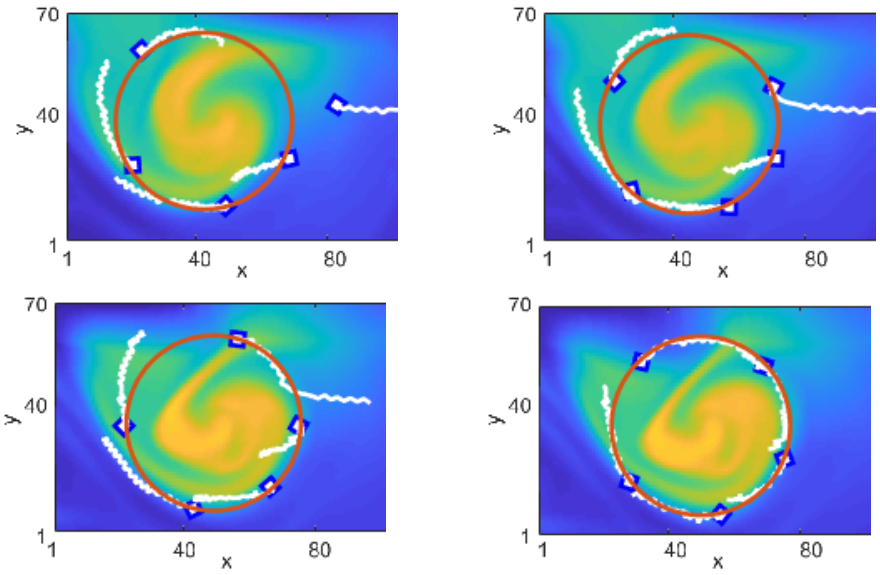

Figure 4.8: Time-lapse of five USVs (blue rectangles) circumnavigating a moving target (red) with representation of their paths (white)

4.5 Summary

In this chapter we considered the problem of multi-vehicle target tracking. We assumed that the target was an irregular dynamic shape approximated by a circle with moving center and varying radius. The difference to the previous chapter is the setup and the protocols designed. We proposed a decentralised estimation protocol in which all agents measure their distance to the boundary, and, by sharing this information, determine the optimal circumnavigation circle.

We defined mathematically this problem by introducing relevant variables and equations that relate them. We also defined the measurements available to each agent as well as the new estimation and circumnavigation objectives. We created a optimal algorithm for estimating the target as well as a control algorithm and we proved their mathematical convergence up to a bound according to our objectives. We presented two simulation results: one to analyse convergence performance and the other to represent the possibility of scaleability regarding introduction of new vehicles of the system, while applying the developed algorithms.

Chapter 5

Cooperative circumnavigation of non-circular shapes

In this chapter we extend the results from Chapter 4 to a more general scenario. We consider circumnavigating irregular non-circular moving shapes. Our goal is to circumnavigate an irregular algal bloom target using a group of vehicles. Each vehicle is equipped with a sensor that indicates its distance to the target's boundary, including whether it is inside or outside of the target. First step is the estimation of the parameters of the algal bloom curvature in each region of the shape, that is, its center and radius for every time instance and for every vehicle. Second step is to design a control law for the vehicles to circumnavigate the shape. We perform a numerical study of the convergence of vehicles to the boundary of the target.

The remaining sections of this chapter are organised as follows. In Section 5.1, the main problem of interest is formulated. The main results are presented in Section 5.2, where the protocol from the previous chapter is extended to arc estimation. Two sets of simulations illustrating the performance of the proposed algorithm are given in Section 5.3. Concluding remarks come in Section 5.4.

5.1 Problem statement

In this chapter we consider the problem of tracking an irregular, moving, and time-varying shape using a multi-vehicle system and a satellite. We see an example of such irregular shape in Fig. 5.1.

An initial image of the algal bloom will begin the mission. The vehicles measure their distance to the target's boundary, as well as whether they are inside or outside the target. Each vehicles shares this information with its two neighboring vehicles. We assume that all vehicle have a common sense of direction with respect to the target, and we assume that every vehicle has one vehicle on the left and on the right. Each vehicle has access to its GPS positions as well as its distance to the boundary of the target and its two neighbours' distances to the target.

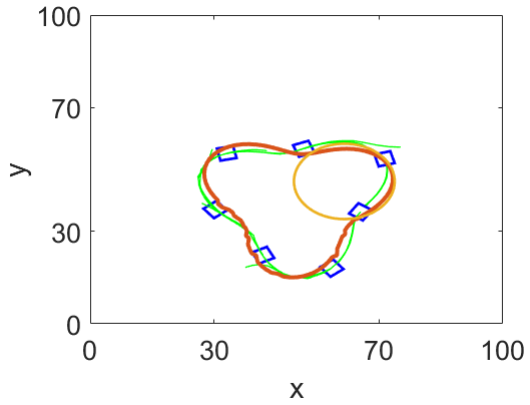

Figure 5.1: Example of an irregular shape with seven vehicles circumnavigating it.

The system of vehicles will circumnavigate the target and provide real-time information of its boundary. We define n vehicles at positions $\mathbf{p}_i(0)$, $i \in [1, \ldots, n]$. They start outside the target and form a counterclockwise undirected ring on the surface. The kinematics of the vehicles is the same as in previous chapters: $\dot{\mathbf{p}}_\mathbf{i} = \mathbf{u}_\mathbf{i}$, $i \in [1, \ldots, n]$ where $\mathbf{p}_i$ is a vector that contains the position $\mathbf{p}_i = [x_i, y_i]^\top \in \mathbb{R}^2$ and $\mathbf{u}_\mathbf{i} \in \mathbb{R}^2$ is the control input.

Each vehicle should define a local curvature through a circle as in Fig.5.1. We define this circle as

$$(\mathbf{c}_\mathbf{i}, r_i) \in \mathbb{R}^3, \tag{5.1}$$

where $\mathbf{c}_\mathbf{i} = (x_i, y_i)$ and r_i are the center and the radius of the circle corresponding to vehicle i.

The distance of each vehicle to the boundary of the target is defined as the smallest measured distance to the boundary, D_i. It is measured by each vehicle. Note that D_i is positive if the vehicle is outside the target and negative if it is inside. We would like to space the vehicles equally along the shape. We can do this by making the distances between vehicles approximately equal. For each vehicle i, its distance to the neighbour in the right $D_{i,i+1}$ and to the neighbour in the left $D_{i,i-1}$:

$$\begin{aligned} D_{i,i+1} &= \|\mathbf{p}_i - \mathbf{p}_{i+1}\|, \qquad i = 1, \ldots, n-1 \\ D_{i,i-1} &= \|\mathbf{p}_i - \mathbf{p}_{i-1}\|, \qquad i = 2, \ldots, n. \\ D_{n,1} = D_{1,n} &= \|\mathbf{p}_n - \mathbf{p}_1\|. \end{aligned} \tag{5.2}$$

5.2 Control strategy and arc estimation

The control architecture is summarised in Fig. 5.2.

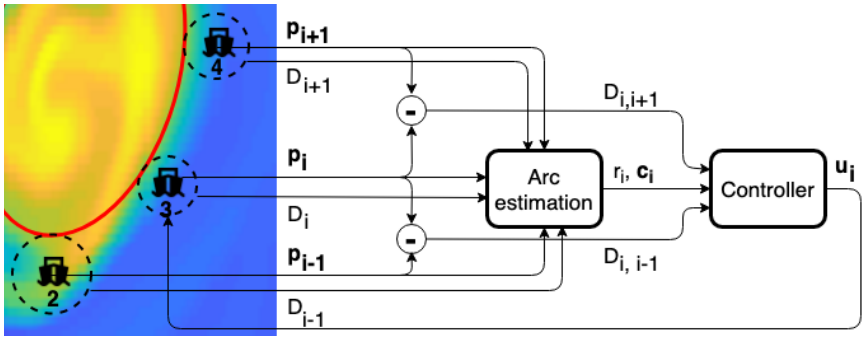

Figure 5.2: Control architecture for vehicle i comunicating with its two neighbours $i-1$ and $i+1$.

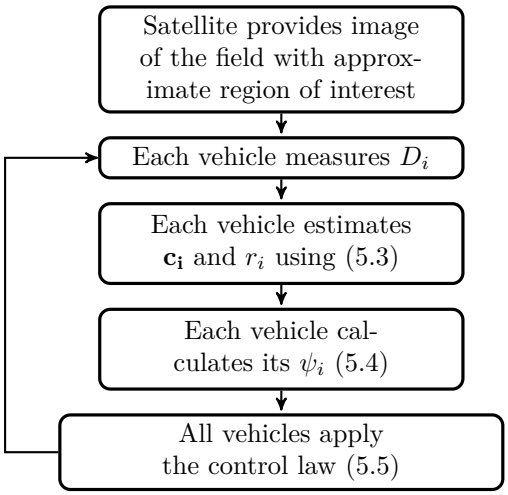

Figure 5.3: Algorithm for positioning the vehicles on the target boundary

We consider n vehicles at positions $\mathbf{p}_i$ and we assume all of them are capable of measuring their distances D_i to the target boundary including whether they are inside (D_i is negative) or outside (D_i is positive) of it. Then, each vehicle estimates $(\mathbf{c_i}, r_i)$ from the shared measurements and positions of its two neighbours. Each vehicle calculates its desired velocity taking into account its distance D_{i+1} and D_{i-1} to its neighbours and its distance to the boundary. The scheme in Fig. 5.3 summarises the algorithm.

First step is the definition of the local circle for each vehicle. Having all the vehicles constantly measuring D_i we fit some shape as in the left image of Fig. 5.4. But, since the target shape is not regular like a circle, we instead define curvatures for every time instance that each vehicle should follow. The curvature for each

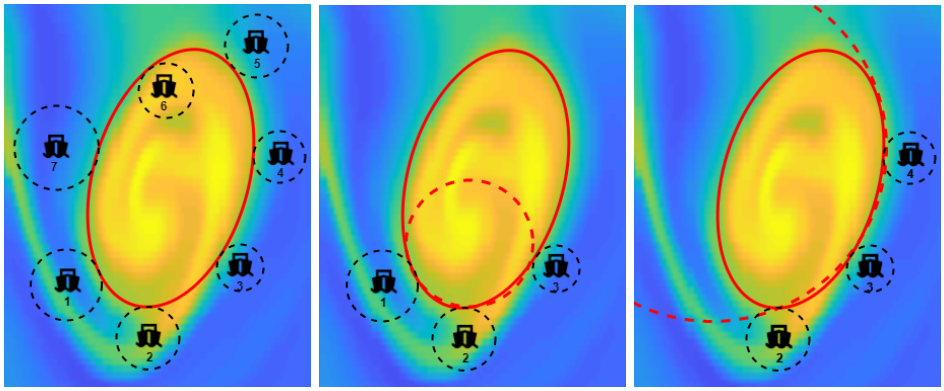

Figure 5.4: Left: 7 vehicles circumnavigate an algal bloom shape (approximately represented by the red oval shape) while measuring their distances to its boundary (dashed black circles) Middle: vehicle 2 communicates with vehicles 1 and 3 to define its ideal curvature (red dashed line) for time instance t. Right: vehicle 3 communicates with vehicles 2 and 4 to define its ideal curvature (red dashed line) for time instance t.

vehicle is defined in a distributed fashion using information of its own and its two neighbours by creating a circle $(\mathbf{c_i}, r_i)$. For example, in the middle image of Fig. 5.4 we can see that vehicle 2 defines a circle using the information of vehicles 1, 2, and 3 while vehicle 3 defines a circle as in the right image of Fig. 5.4 using the information of vehicles 2, 3, and 4. Each vehicle estimates its circle from

$$\begin{aligned} &\min_{\mathbf{c_i}, r_i} \sum_{k=i-1}^{i+1} \left(\|\mathbf{p}_k - \mathbf{c_i}\| - (r_i + D_k)\right)^2, \qquad i = 1, \ldots, n. \\ &s.t \qquad r > 0. \end{aligned} \tag{5.3}$$

Now, we want to obtain the desired control input $\mathbf{u_i}$ using the measured and estimated variables. The total velocity of each vehicle comprises of parts: approaching the target and circumnavigating it. Therefore we define the direction of each vehicles towards the center of the target as the bearing,

$$\psi_i = \frac{\mathbf{c_i} - \mathbf{p}_i}{\|\mathbf{c_i} - \mathbf{p}_i\|}. \tag{5.4}$$

The control law for each vehicle i is

$$\mathbf{u_i} = D_i \psi_i + \frac{D_{i,i+1}}{D_{i,i-1}} E \psi_i \tag{5.5}$$

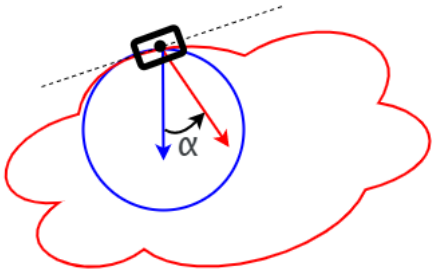

Figure 5.5: Representation of the angle α between the normal vector to the circle (blue) and the normal vector to the target (red) at the vehicle's location (black square and dot).

5.3 Numerical results

In this section, we present simulations for the protocol designed in Section 5.2. In the first subsection we apply our protocol to a slowly drifting and shape-shifting ellipsoid and in the second subsection we apply it to a static yet irregular shape that looks like a three-leafed clover.

We define the angle α between the normal vector to the circle and the normal vector to the target at the vehicle's location as in Fig. 5.5. Note that, as seen in this figure, a perfect estimate corresponds to $\alpha = 0$.

5.3.1 Oval shape with five vehicles

We first simulate a moving target with initial position $(x[0], y[0]) = (50, 40)$, horizontal radius $r_h[0] = 25$, vertical radius $r_v[0] = 15$. The shape evolves with the following dynamics

$$\begin{aligned} x[t+1] &= x[t] + \gamma_1[t] + 0.2 \\ y[t+1] &= y[t] + \gamma_2[t] + 0.2 \\ r_h[t+1] &= r_h[t] + \gamma_3[t] + 0.2 \\ r_v[t+1] &= r_v[t] + \gamma_4[t] + 0.2. \end{aligned} \tag{5.6}$$

We assume that each vehicle has access to a common initial noisy estimate of $(\hat{x}[0], \hat{y}[0]) = (50, 40)$, radius $\hat{r}[0] = 25$. Note that at time $t = 0$ the radius estimate is equal to the ellipsoid's largest radius. Here, $\gamma_i[t]$ is a random scalar drawn from the uniform distribution within the interval $[-0.5, 0.5]$ for $i = 1, \ldots, 4$.

Fig. 5.6 shows the multi-vehicle system converges towards the moving target. The red ellipsoid is the target shape, the blue squares are the vehicles and the green lines are the path each vehicle took. Fig. 5.7 illustrates the idea of how the USVs estimate and track the target. Here the yellow circle is the circle estimate of one of the vehicles. As shown, the estimated circle of vehicle i partially coincides with the target, in the neighboring region of vehicle i. We can see that the trajectories closely match the target shape.

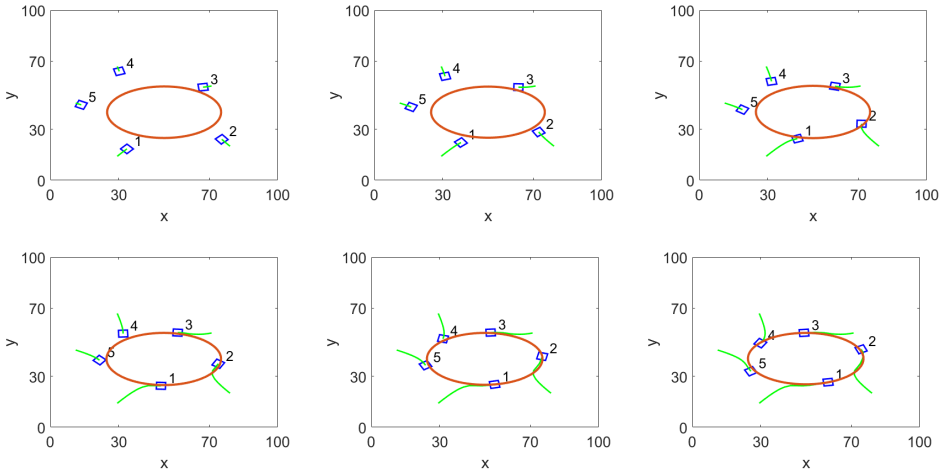

Figure 5.6: Time-lapse of five USVs (blue rectangles) converging and starting to circumnavigate a moving target (red) with representation of their paths (green).

Fig. 5.8 shows a detailed analysis of this case study. The top two figures compare the ellipse target to the estimated circle for vehicle 1. This comparison comprises of the center with x and y parameters. We can see that the center is, on average, close to the ellipsoid's center. Second row shows the time evolution of $\cos(\alpha)$, the angle between the normal vectors to the surface of both the ellipse and the circle. Note that the normal vector to the surface of the circle ψ_1 is used by each vehicle. If the estimation protocol was perfect, it should be equal to the normal vector to the target. This corresponds to $\alpha = 0$. The figure shows that the estimated normal vector is mostly close to the target's normal vector.

The left plot in the third row shows the distance of vehicle 1 to the boundary of the target, D_1. The vehicle starts far from the target and quickly converges towards its boundary. As the target itself moves and changes size and shape, the vehicle will constantly adjust it's trajectory to go towards the boundary. This creates the observed ripple in the plot.

Third row right plot shows the ratio of two distances: the distance of vehicle 1 to the neighboring vehicles n and 2. As expected this ratio is close to one. On the last row, we have the control input for vehicle 1. Note that the oscillation corresponds to a turn around the target.

5.3.2 Irregular shape with seven vehicles

We first simulate a static target shape with static position $(x, y) = (50, 40)$ and radius $r(\theta) = 5\sin(0.06\pi\theta) + 20$. We assume that each vehicle has access to a common initial noisy estimate of $(\hat{x}[0], \hat{y}[0]) = (50, 40)$, radius $\hat{r}[0] = 20$. Note that

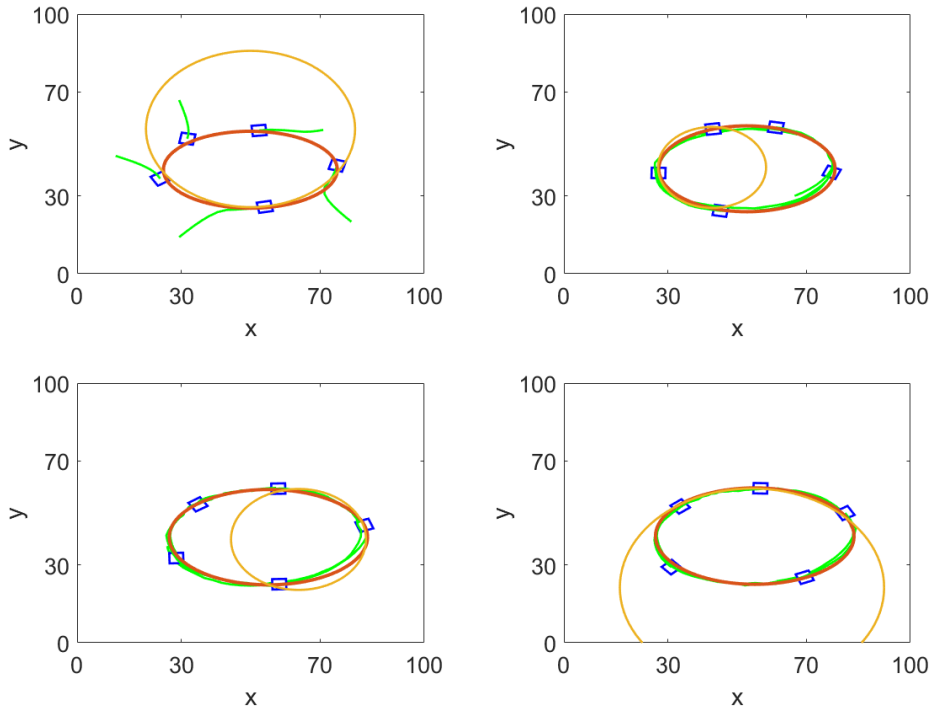

Figure 5.7: Time-lapse of five USVs (blue rectangles) circumnavigating a moving target (red) with the estimated circle of one of them (yellow), and representation of their paths (green)

at time $t = 0$ the radius estimate is equal to the shape's average radius. We use seven vehicles to track this target.

Fig. 5.9 presents the convergence towards the target. Fig. 5.10 shows, similarly to Fig. 5.7, how a local circle is used to compute the control. The plots indicate that the protocols perform well and that there is some oscillations due to the target shape. A more detailed analysis is given in Fig. 5.11. The top two plots show that the center is, on average, close to the target's center, and oscillating around it.

5.4 Summary

In this chapter we considered the problem of multi-vehicle target tracking of irregular dynamic shapes. The problem statement of Chapter 4 was extended by adapting its control and estimation protocol to a more generic scenario. We proposed a decentralised estimation protocol in which all vehicles measure their distance to the

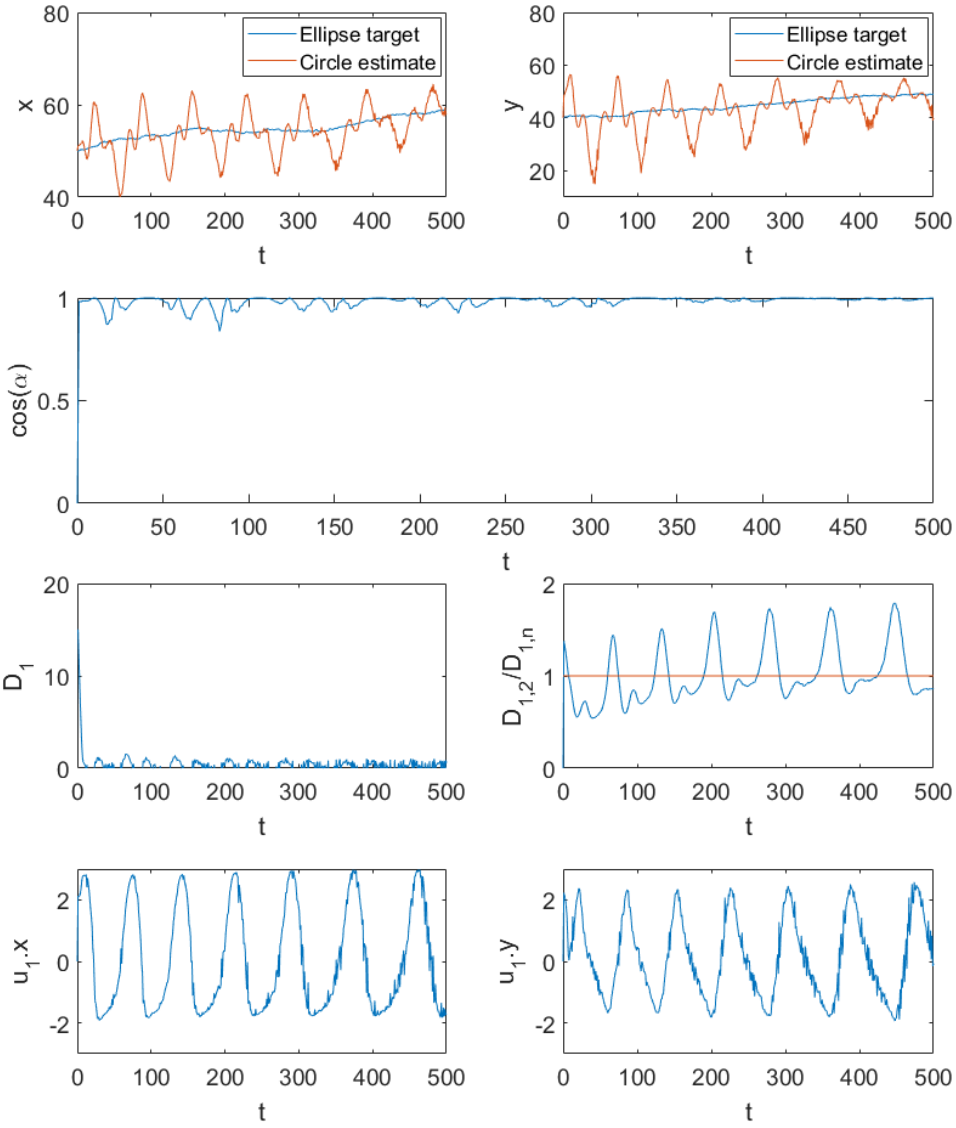

Figure 5.8: First row: target and estimated circle's center $\mathbf{c} : x, y$. Second row: Cosine of the angle between the normals to the target and circle $\cos(\alpha)$. Third row: tracking error of USV A_1, D_1 and ratio between vehicle's distances $D_{1,2}/D_{1,n}$. Fourth row: control input of USV A_1, $\mathbf{u_1} : x, y$

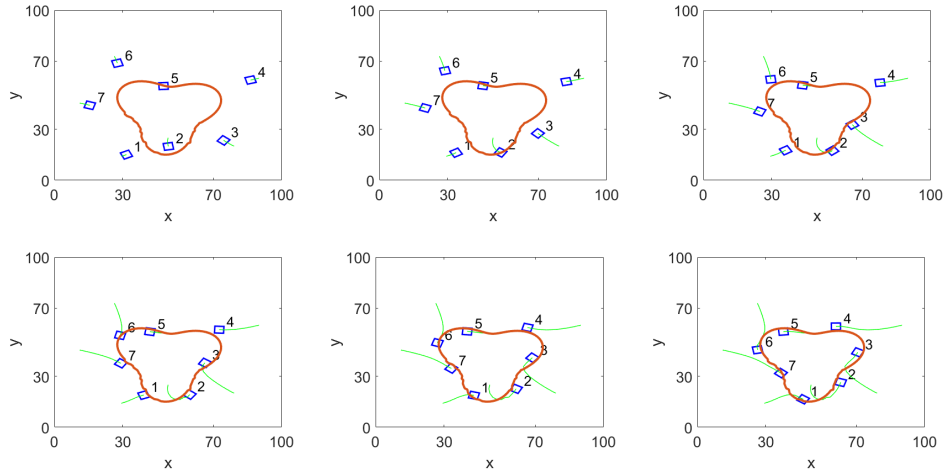

Figure 5.9: Time-lapse of five USVs (blue rectangles) converging and starting to circumnavigate a moving target (red) with representation of their paths (green).

boundary. It was assumed that the vehicles share this information with their two neighbours and each vehicle determines a circle that best approximates the curvature on the vehicle's area. We presented two numerical simulation results: one using a dynamic oval shape and one using a non-circular static shape. For both simulations our algorithm was successful as we observed convergence with bounded and small tracking errors. The second simulation had bigger tracking errors than the first. This outcome is expected since the protocol relies on neighbor information for estimation, and so, the more irregular a shape is, the more vehicles are needed to accurately estimate it.

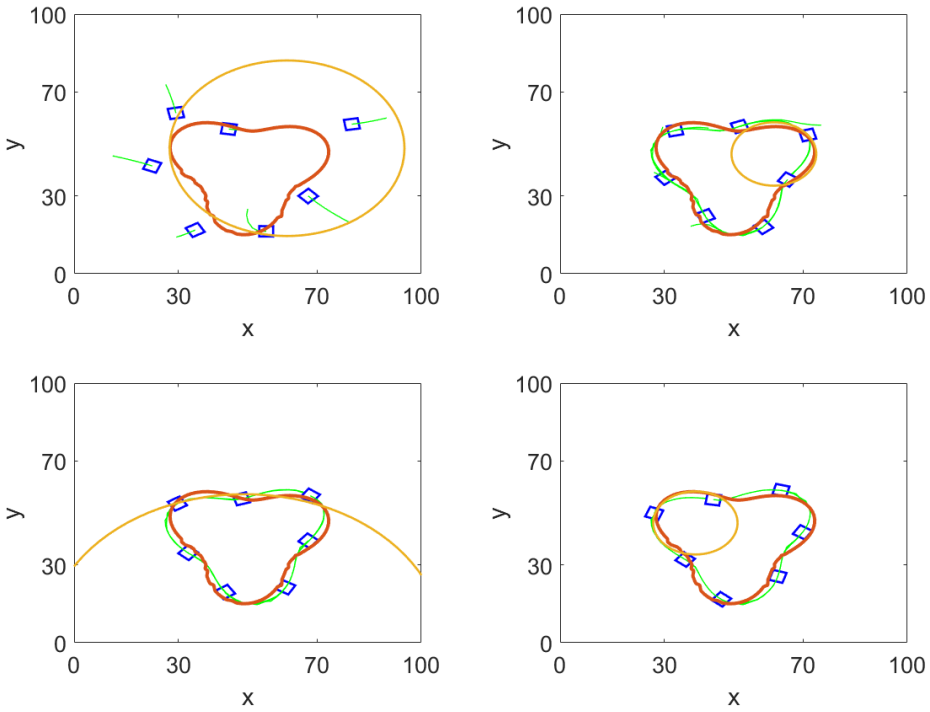

Figure 5.10: Time-lapse of seven USVs (blue rectangles) circumnavigating a static target (red) with representation of their trajectories (green) and the estimated circle of one of them (yellow).

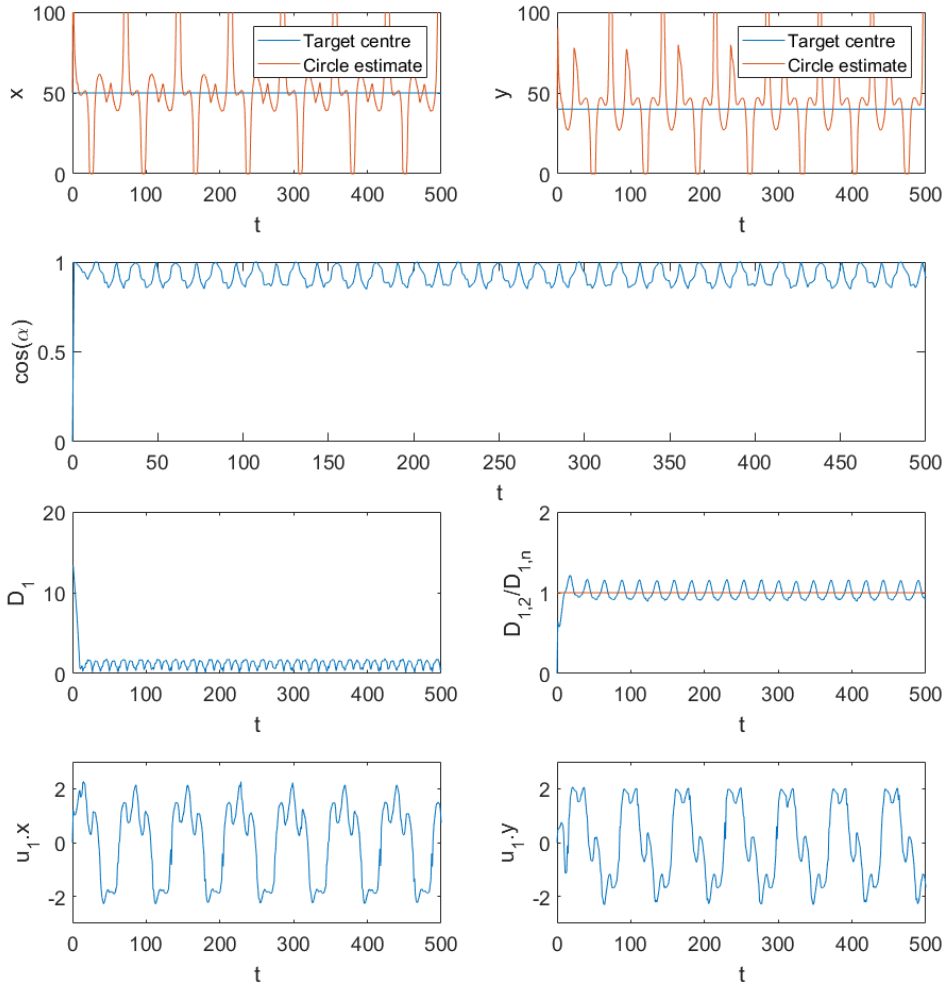

Figure 5.11: First row: target and estimated circle's center $\mathbf{c} : x, y$. Second row: Cosine of the angle between the normals to the target and circle $\cos(\alpha)$. Third row: USV A_1's distance to the boundary D_1 and ratio of distances between neighbours $\frac{D_{1,2}}{D_{1,n}}$. Fourth row: control input of USV A_1, $\mathbf{u_1} : x, y$.

Chapter 6

Conclusions

In this chapter we conclude the thesis. In Section 6.1 we summarise and discuss the presented results, and in Section 6.2 outline some possible extensions and future work.

6.1 Summary

The central question of this thesis was how can we use a cooperative system of USVs paired with a satellite to estimate, track, and circumnavigate a mobile, irregular, and of varying size target. We defined two estimation and control protocols. We proved convergence of the two protocols and provided some simulation examples.

In Chapter 3 we considered the problem of tracking a mobile target using adaptive estimation while circumnavigating it with a set of USVs. The mobile target considered is an irregular dynamic shape approximated by a circle with moving center and varying radius. The USV system is composed of n USVs and we assume that one USV measures the distance to the boundary and to the center of the target. This mesurement can be done if, for example, this USV is equipped with an UAV. This USV uses adaptive estimation to calculate the location and size of the mobile target. The USV system must circumnavigate the boundary of the target while forming a regular polygon. We designed two algorithms: One for the adaptive estimation of the target using the UAV's measurements and another for the control protocol to be applied by all USVs in their navigation. The convergence of both algorithms to the desired state wass proved up to a limit bound. Two simulated examples were provided to verify the performance of the algorithms designed.

In Chapter 4 we proposed a reliable method to track algal blooms using a set of USVs. A satellite image indicates the existence and initial location of the algal bloom for the deployment of the robot system. The algal bloom area is approximated by a circle with time-varying location and size. This circle is estimated and circumnavigated by the robots which are able to locally sense its boundary. A multi-agent control algorithm is proposed for the continuous monitoring of the

evolution of the algal bloom. The algorithm is comprised of a decentralised least squares estimation of the target and a controller for circumnavigation. We proved the convergence of the robots to the circle and equally spaced positions around it. Simulation results with data provided by the SINMOD ocean model were used to illustrate the theoretical results.

In Chapter 5 we considered the problem of tracking an irregular shape using a decentralised system of vehicles as well as circumnavigating such shape. Like in the previous chapter, we used a protocol based on decentralised least-squares estimation. Each vehicle is able to communicate with only the nearest neighbours, thus forming an undirected ring graph. We assumed that each vehicle measures its distance to the boundary of the target as well as whether it is inside or outside such target. The convergence of both algorithms to the desired state was proven up to a limit bound. Two simulated examples were provided to verify the performance of the algorithms designed.

6.2 Future work

There are many challenging open questions in the topic of multi-vehicle circumnavigation and target tracking. In this section, we discuss some natural extensions of the work presented in this thesis. The proposed extensions are to include more detailed dynamic models for the vehicles as well as the environment, to improve the estimation algorithm by employing the satellite data, to analyse convergence of the protocol in Chapter 5, and to evaluate the approach on a realistic simulation platform and on real vehicles.

Motivated by the desire to develop better control laws, we plan on using a more detailed USV model. In the work presented in this thesis, we considered each vehicle as a unit point with simple integrator dynamics. We plan on using a dynamical USV model and then addapt our protocols. We will focus on non-holonomic models and start by using the unicycle model for disturbance rejection [41] and robust consensus [42]. Furthermore, by introducing environmental uncertainties we will make our control laws more robust. We will introduce wind, wave and ocean forces as modelled in [43]. Currently, we assume that our vehicles encounter no challenges in reaching their desired trajectories. By introducing these perturbances, we can create a lower-level control that can guarantee path following.

We plan to solve the estimation fusion problem using both local and global data: from the satellite and from local vehicle measurements. Currently, we estimate the target using only local measurements and we use the satellite for deployment and estimate initialisation. The estimates we get from local measurements are more accurate and frequent than global satellite imaging. We believe that, by pairing a local and a global estimation protocol, we will be able to substantially improve our current tracking and estimation results. This can be done using the novel approach of data assimilation. Ocean data assimilation is increasingly recognized as crucial for the accuracy of real-time oceanic prediction systems [44].

In Chapter 5 we presented an extension of the protocol from Chapter 4. A logical next step is to analyse the system and study under which assumption it converges to the desired state.

In order to validate of our results, we plan to employ more realistic simulation tools. One example is to use platforms that take into consideration ocean dynamics including currents, waves, and fluctuation such as Neptus [45]. Finally, implementation on a real vehicle system is an important next step.

List of Figures

Bibliography

[1] SMHI satellite data on algae. https://www.smhi.se/data/oceanografi/algsituationen. Accessed: 2020-02-08.

[2] S. Shumway, J. Burkholder, and S. Morton, *Harmful Algal Blooms: A Compendium Desk Reference*. John Wiley & Sons, 2018.

[3] M. L. Wells, V. L. Trainer, T. J. Smayda, B. S. Karlson, C. G. Trick, R. M. Kudela, A. Ishikawa, S. Bernard, A. Wulff, D. M. Anderson, and W. P. Cochlan, "Harmful algal blooms and climate change: Learning from the past and present to forecast the future," *Harmful Algae*, vol. 49, pp. 68 – 93, 2015.

[4] P. Wassmann, D. Slagstad, C. W. Riser, and M. Reigstad, "Modelling the ecosystem dynamics of the barents sea including the marginal ice zone: II. carbon flux and interannual variability," *Journal of Marine Systems*, vol. 59, no. 1, pp. 1 – 24, 2006.

[5] P. J. S. Franks, "Recent advances in modelling of harmful algal blooms," in *Global Ecology and Oceanography of Harmful Algal Blooms*. Springer International Publishing, 2018, pp. 359–377.

[6] SMHI algal bloom report from satellite. https://www.smhi.se/kunskapsbanken/oceanografi/algblomning-1.1734, Updated July 23, 2018; published June 24, 2011.

[7] M. Johansen. (July 2019) Algal report number 7, 2019. https://www.smhi.se/publikationer/publikationer/algrapporter/algrapport-nummer-7-2019-1.150075.

[8] R. Ringbäck, "Multi-agent autonomous target tracking using distance-based formations," Master's thesis, Automatic Control, Royal Institute of Technology, Sweden, 2017.

[9] A. Sivertsen, S. Solbø, R. Storvold, A. Tøllefsen, and K.-S. Johansen, "Automatic mapping of sea ice using unmanned aircrafts," *ReCAMP Flagship Workshop Book of Abstracts*, p. 30, 2016.

[10] J. B. de Sousa and F. L. Pereira, "On the future of ocean observation," in *O mar no futuro de Portugal: Ciência e visão estratégica.* Lisboa: Centro de estudos estratégicos do Atlântico, 2014.

[11] A. Lucieer, D. Turner, D. H. King, and S. A. Robinson, "Using an unmanned aerial vehicle (UAV) to capture micro-topography of antarctic moss beds," *International Journal of Applied Earth Observation and Geoinformation*, vol. 27, pp. A:53 – 62, 2014.

[12] A. Zolich, D. Palma, K. Kansanen, K. Fjørtoft, J. Sousa, K. H. Johansson, Y. Jiang, H. Dong, and T. A. Johansen, "Survey on communication and networks for autonomous marine systems," *Journal of Intelligent & Robotic Systems*, Apr 2018.

[13] R. Millet, F. Plumet, and J. Dern, "Autonomous surface vehicle for oceanographic survey," *International Autonomous Surface Ship Symposium*, Jan 2008.

[14] LSTS website. https://www.lsts.pt. Accessed: 2020-01-15.

[15] R. M. Murray, "Recent Research in Cooperative Control of Multivehicle Systems," *Journal of Dynamic Systems, Measurement, and Control*, vol. 129, no. 5, pp. 571–583, May 2007.

[16] Y. Cao, W. Yu, W. Ren, and G. Chen, "An overview of recent progress in the study of distributed multi-agent coordination," *IEEE Transactions on Industrial Informatics*, vol. 9, no. 1, pp. 427–438, Feb 2013.

[17] M. Egerstedt and X. Hu, "Formation constrained multi-agent control," *IEEE transactions on robotics and automation*, vol. 17, no. 6, pp. 947–951, 2001.

[18] I. Shames, B. Fidan, and B. D. O. Anderson, "Close target reconnaissance using autonomous uav formations," in *2008 47th IEEE Conference on Decision and Control*, Dec 2008, pp. 1729–1734.

[19] D. V. Dimarogonas and K. H. Johansson, "On the stability of distance-based formation control," in *the Proceedings of the 47th IEEE Conference on Decision and Control*. IEEE, 2008, pp. 1200–1205.

[20] M. Cao, A. S. Morse, C. Yu, B. D. O. Anderson, and S. Dasgupta, "Controlling a triangular formation of mobile autonomous agents," in *the Proceedings of the 46th IEEE Conference on Decision and Control*. IEEE, 2007, pp. 3603–3608.

[21] Z. Sun, *Cooperative Coordination and Formation Control for Multi-agent Systems*, ser. Springer Theses Series. Springer International Publishing, 2018.

[22] M. Ani Hsieh, V. Kumar, and L. Chaimowicz, "Decentralized controllers for shape generation with robotic swarms," *Departmental Papers (MEAM)*, vol. 26, Sept 2008.

[23] G. Li, D. St-Onge, C. Pinciroli, A. Gasparri, E. Garone, and G. Beltrame, "Decentralized progressive shape formation with robot swarms," *Autonomous Robots*, pp. 1–17, Oct 2018.

[24] N. E. Leonard, D. A. Paley, F. Lekien, R. Sepulchre, D. M. Fratantoni, and R. E. Davis, "Collective motion, sensor networks, and ocean sampling," *Proceedings of the IEEE*, vol. 95, no. 1, pp. 48–74, Jan 2007.

[25] G. Gu, P. R. Chandler, C. J. Schumacher, A. Sparks, and M. Pachter, "Optimal cooperative sensing using a team of uavs," *IEEE Transactions on Aerospace and Electronic Systems*, vol. 42, no. 4, pp. 1446–1458, Oct 2006.

[26] A. S. Matveev, H. Teimoori, and A. V. Savkin, "Range-only measurements based target following for wheeled mobile robots," *Automatica*, vol. 47, pp. 177–184, 2011.

[27] I. Shames, S. Dasgupta, B. Fidan, and B. D. O. Anderson, "Circumnavigation using distance measurements under slow drift," *IEEE Transactions on Automatic Control*, vol. 57, no. 4, pp. 889–903, 2012.

[28] A. S. Matveev and K. S. Ovchinnikov, "Distributed communication-free control of multiple robots for circumnavigation of a speedy unpredictably maneuvering target," *the Proceedings of 2018 European Control Conference (ECC)*, pp. 1797–1802, 2018.

[29] R. Zheng and D. Sun, "Circumnavigation by a mobile robot using bearing measurements," *2014 IEEE/RSJ International Conference on Intelligent Robots and Systems*, pp. 4643–4648, 2014.

[30] M. Deghat, L. Xia, B. D. O. Anderson, and Y. Hong, "Multi-target localization and circumnavigation by a single agent using bearing measurements," *International Journal of Robust and Nonlinear Control*, vol. 25, no. 14, pp. 2362–2374, 2015.

[31] A. Boccia, A. Adaldo, D. V. Dimarogonas, M. di Bernardo, and K. H. Johansson, "Tracking a mobile target by multi-robot circumnavigation using bearing measurements," in *the Proceedings of IEEE 56th Annual Conference on Decision and Control, CDC 2017*, ser. IEEE Conference on Decision and Control. IEEE, 2017, pp. 1076–1081.

[32] J. O. Swartling, I. Shames, K. H. Johansson, and D. V. Dimarogonas, "Collective circumnavigation," *Unmanned Systems*, vol. 02, no. 03, pp. 219–229, 2014.

[33] M. Deghat, E. Davis, T. See, I. Shames, B. D. O. Anderson, and C. Yu, "Target localization and circumnavigation by a non-holonomic robot," in *Proceedings of the IEEE/RSJ International Conference on Intelligent Robots and Systems.*, Oct 2012, pp. 1227–1232.

[34] A. Franchi, P. Stegagno, and G. Oriolo, "Decentralized multi-robot encirclement of a 3D target with guaranteed collision avoidance," *Autonomous Robots*, vol. 40, Jul 2015.

[35] B. D. O. Anderson, "Exponential stability of linear equations arising in adaptive identification," *IEEE Transactions on Automatic Control*, vol. 22, no. 1, pp. 83–88, 1977.

[36] N. Shimkin and A. Feuer, "Persistency of excitation in continuous-time systems," *Systems & Control Letters*, vol. 9, no. 3, pp. 225 – 233, 1987.

[37] L. Farina and S. Rinaldi, *Positive Linear Systems: Theory and Applications*, ser. A Wiley-Interscience publication. Wiley, 2000.

[38] J. Wei, X. Yi, H. Sandberg, and K. H. Johansson, "Nonlinear consensus protocols with applications to quantized communication and actuation," *IEEE Transactions on Control of Network Systems*, 2018.

[39] K. J. Åström, "Adaptive control," in *Mathematical System Theory: The Influence of R. E. Kalman*, A. C. Antoulas, Ed. Springer Berlin Heidelberg, 1991, pp. 437–450.

[40] SINMOD simulation data. https://www.sintef.no/en/ocean/initiatives/sinmod/. Accessed: 2020-01-30.

[41] M. Jafarian, E. Vos, C. De Persis, J. Scherpen, and A. van der Schaft, "Disturbance rejection in formation keeping control of nonholonomic wheeled robots," *International Journal of Robust and Nonlinear Control*, vol. 26, no. 15, pp. 3344–3362, 2016.

[42] M. Jafarian, "Robust consensus of unicycles using ternary and hybrid controllers," *International Journal of Robust and Nonlinear Control*, vol. 27, no. 17, pp. 4013–4034, 2017.

[43] T. I. Fossen, *Handbook of Marine Craft Hydrodynamics and Motion Control.* John Wiley & Sons, Ltd, May 2011.

[44] A. M. Moore, M. J. Martin, S. Akella, H. G. Arango, M. Balmaseda, L. Bertino, S. Ciavatta, B. Cornuelle, J. Cummings, S. Frolov, P. Lermusiaux, P. Oddo, P. R. Oke, A. Storto, A. Teruzzi, A. Vidard, and A. T. Weaver, "Synthesis of ocean observations using data assimilation for operational, real-time and reanalysis systems: A more complete picture of the state of the ocean," *Frontiers in Marine Science*, vol. 6, p. 90, 2019.

[45] NEPTUS command and control software developed by LSTS. https://lsts.fe.up.pt/toolchain/neptus. Accessed: 2020-02-12.